

**SINGLE-CELL ELECTROPORATION USING ELECTROLYTE-FILLED  
CAPILLARIES WITH MICRO-SCALE TIPS**

by

**Manyan Wang**

BS, Nankai University, China 2000

MS, Nankai University, China 2003

Submitted to the Graduate Faculty of  
Art and Science in partial fulfillment  
of the requirements for the degree of  
Master of Science

University of Pittsburgh

2008

UNIVERSITY OF PITTSBURGH  
SCHOOL OF ART AND SCIENCE

This thesis was presented

by

Manyan Wang

It was defended on

Jan. 14<sup>th</sup>, 2008

and approved by

Stephen G. Weber, Professor, Department of Chemistry

Adrian Michael, Associate Professor, Department of Chemistry

Shigeru Amemiya, Assistant Professor, Department of Chemistry

Thesis Director: Stephen G. Weber, Professor, Department of Chemistry

Copyright © by Manyan Wang

2008

# **SINGLE-CELL ELECTROPORATION USING ELECTROLYTE-FILLED CAPILLARIES WITH MICRO-SCALE TIPS**

Manyan Wang, M.S.

University of Pittsburgh, 2008

Single-cell electroporation (SCEP) is a recently developing powerful technique for cell analysis and cell manipulation. In the first chapter of this thesis, a review about the theories and techniques is fulfilled, including a detailed description of the factors affecting SCEP, and a discussion about how to optimize SCEP for high efficiency and survivability. Based on the previous experimental results and numerical simulation, a hypothesis is proposed which leads us to find that small tips could be a solution to electroporate small cells with simultaneous maximization of electroporation efficiency and survivability when using electrolyte-filled capillaries (EFC) with pulled tips.

In the second chapter, an integrated circuit for SCEP and controlling is demonstrated. EFCs with 2  $\mu\text{m}$  tips are constructed and used for SCEP of A549 cells with an extremely high spatial resolution. Distance between tip and cell is revealed to be vital in SCEP because of its direct control of the local electric field distribution and strength; to control distance precisely, a current measurement method inspired by tip-cell giga-seals is applied. High temporal resolution videos hint an abrupt intracellular fluorescence loss at the time scale of pulse duration followed by recovery in the small portion of cell membrane facing the tips. Viability of cells is highly related to the fluorescence loss, fluorescence exposure and dye types. Comsol simulation using the real shape capillaries helps to guide the electroporation throughout our experiments.

However, this protocol evokes overcoming technical difficulties in terms of getting high survivability and decreasing variance, which are our two main aims. The advantage of small tips and the hypothesis are still to be examined. This is referred in the third chapter, as well as other following-up future work.

## TABLE OF CONTENTS

PREFACE.....	XIV
1.0 INTRODUCTION OF SINGLE-CELL ELECTROPORATION.....	1
1.1 INTRODUCTION OF ELECTROPORATION.....	1
1.1.1 What is electroporation .....	1
1.1.2 Basic electroporation notions.....	3
1.1.2.1 Transmembrane potential.....	3
1.1.2.2 Polarization of cells in external electric field.....	4
1.1.2.3 Critical transmembrane potential ( $TMP_c$ ) for electroporation .....	5
1.1.2.4 Kinetic description of reversible electroporation.....	6
1.1.3 Important parameters in electroporation .....	7
1.1.3.1 Electrical parameters.....	8
1.1.3.2 Cellular factors .....	10
1.1.3.3 Physicochemical factors.....	12
1.1.4 Brief introduction to mechanism study of electroporation .....	14
1.1.4.1 The mechanism of electroporation remains unclear .....	14
1.1.4.2 Pores.....	14
1.2 PROGRESS IN SINGLE-CELL ELECTROPORATION (SCEP).....	16
1.2.1 Why study single-cell electroporation? .....	16

1.2.2	SCEP with solid microelectrodes.....	17
1.2.3	SCEP with patch micropipette and capillaries.....	19
1.2.3.1	Micropipet.....	19
1.2.3.2	Electrolyte-filled capillaries (EFC).....	23
1.2.4	SCEP with microfabricated chips.....	25
1.2.5	Other techniques for SCEP: multi-walled carbon nanotubes .....	31
1.2.6	Single-cell analysis and SCEP .....	32
1.2.7	Optimization of SCEP for high efficiency and survivability.....	34
1.2.7.1	Larger variance in SCEP than in bulk electroporation .....	34
1.2.7.2	Distance is a vital factor for electric field distribution.....	35
1.2.7.3	Small-sized cell is a challenge .....	37
1.2.7.4	Our hypothesis of cell electroporation and survivability .....	38
2.0	SCEP WITH EFC MICRO-TIPS.....	41
2.1	INTRODUCTION: SMALLER TIP SIZE OF EFC MAY SOLVE THE PROBLEM OF SMALL-SIZED CELLS.....	41
2.2	MATERIALS AND METHODS .....	43
2.2.1	Materials.....	43
2.2.2	Cell culture and preparation.....	43
2.2.3	Cell fluorescence staining.....	44
2.2.3.1	Staining for SCEP observation .....	44
2.2.3.2	Cell viability check .....	45
2.2.4	EFC fabrication and buffer filling .....	46
2.2.5	Microscope imaging.....	47

2.3	INSTRUMENTATION FOR SCEP WITH EFC .....	48
2.3.1	Circuit design and electronics .....	48
2.3.1.1	Electroporation circuit.....	49
2.3.1.2	Test circuit.....	50
2.3.2	EFC resistance.....	51
2.3.3	Current measurement controlled tip-cell distance .....	52
2.4	NUMERICAL SIMULATION.....	54
2.4.1	Model setup and parameters .....	54
2.4.1.1	Capillary drawing in Comsol .....	54
2.4.1.2	Model and parameters.....	56
2.4.2	Potential and electric field distribution near the EFC tip.....	57
2.4.3	Resistance for EFC with different tip size .....	59
2.4.4	Resistance with cells at various tip-cell distances.....	60
2.4.5	FEA and TMP for electroporation.....	62
2.5	ELECTROSMOTIC FLOW DURING ELECTROPORATION .....	63
2.6	ELECTROPORATION RESULT.....	66
2.6.1	Excellent spatial resolution.....	66
2.6.2	Fluorescence exposure and dye selection affect cell viability .....	67
2.6.3	SCEP with Propidium Iodide staining .....	68
2.6.4	Fast temporal resolution imaging .....	69
2.6.5	Technical issue limits distance control and small tips.....	70
2.6.5.1	Preliminary electroporation results .....	70
2.6.5.2	Capillary reproducibility .....	73

2.6.5.3	Micromanipulator backlash.....	73
2.7	CONCLUSIONS .....	74
3.0	FUTURE WORK.....	75
3.1	CONTINUE WORK ON SURVIVABILITY AND VARIANCES PROBLEM	75
3.1.1	Piezo actuator for distance control.....	75
3.1.2	Temperature control by PDMI-2 micro-incubator .....	75
3.1.3	Cell Synchronization.....	76
3.1.4	Working on other parameters .....	76
3.2	DYNAMIC AND PORE INFORMATION STUDY .....	77
3.3	SECP OF OTHER CELL LINES .....	77
	BIBLIOGRAPHY.....	78

## LIST OF TABLES

Table 1. 1: Comparison of most commonly used techniques of signal generation for electroporation [1].....	10
Table 2. 1: Programs for capillary pulling .....	47
Table 2. 2: Parameters and constants .....	56
Table 2. 3: Simulated resistance of different tip-sized capillaries at different temperature .....	60
Table 2. 4: Resistance measurement in electroporation simulation model with small cells ( $R = 10 \mu\text{m}$ ) and $2 \mu\text{m}$ tip EFC .....	61
Table 2. 5: Short distance resistance measurement in electroporation simulation model with large cells ( $R = 20 \mu\text{m}$ ) and $2 \mu\text{m}$ tip EFC.....	62
Table 2. 6: Summary of cell electroporation success and survival results at $d = 3.5 \mu\text{m}$ .....	67
Table 2. 7: Success and viability in SCEP with different cell sizes and shapes .....	72

## LIST OF FIGURES

Figure 1. 1: Exposure of a cell to an electric field may result in either permeabilization of cell membrane or its destruction.....	2
Figure 1. 2: Polarization of a cell in external electric field.....	5
Figure 1. 3: Role of electric field on electroporation.....	8
Figure 1. 4: Cell cycle.....	11
Figure 1. 5: Hypothetical bilayer membrane structural rearrangements.....	15
Figure 1. 6: (A) SCEP with two carbon fiber microelectrodes; (B) Combining with patch clamp technique.....	19
Figure 1. 7: Electroinjection of fluorescein into a giant unilamellar vesicle with a microelectrode and injection micropipette.....	20
Figure 1. 8: SCEP of slices with micropipette.....	21
Figure 1. 9: Illustration of the modified SCEP-mediated transfection setup.....	22
Figure 1. 10: SCEP with EFC: schematic picture of the experimental setup.....	24
Figure 1. 11: First SCEP microchip.....	27
Figure 1. 12: Layout of the chip and cell.....	28
Figure 1. 13: Schematic view of the electroporation device.....	28
Figure 1. 14: $\mu$ PREP chip.....	29

Figure 1. 15: The phase diagram for electroporation and cell lysis. (A) PI uptake in cabbage cells, (B) electroporation of Hela cells with four different sizes of dextrans. ....	30
Figure 1. 16: TEM image of CNT electroporation .....	31
Figure 1. 17: Whole-cell fluorescence intensity vs. time during electroporation of single A549 cells. ....	35
Figure 1. 18: Determination of optimal parameters to achieve maximum cell survivability and electroporation .....	36
Figure 1. 19: Contour plots of probabilities of cell survivability and electroporation success as a function of pulse duration and cell-capillary tip distance and cell properties .....	38
Figure 1. 20: Simulated FEA, Maximum TMP and electroporated area plotted as a function of distance for different sized cells.. ....	39
Figure 2. 1: FEA and Maximum TMP plotted as a function of distance for different sized cells at 25 °C. ....	42
Figure 2. 2: Comparison of 2 μm and 3.6 μm tips regarding FEA and maximum TMP for different sized cells at 25 °C.. ....	42
Figure 2. 3: Pictures of pulled capillaries under microscope (40×).. ....	47
Figure 2. 4: Schematic diagram of the experimental setup. ....	49
Figure 2. 5: Resistance changes when a 5 μm capillary tip seals with cell membrane.....	53
Figure 2. 6: SCEP modeling geometry. ....	55
Figure 2. 7: Simulated electric field and potential distribution. ....	58
Figure 2. 8: A picture of fluorescent-beads-filled capillary for electroosmotic flow study .....	64

Figure 2. 9: Fluorescence intensity change within the focused tip portion when pulses are applied on the fluorescent-beads-filled capillaries..	64
Figure 2. 10: High spatial resolution of electroporation with a 2 $\mu\text{m}$ tip EFC..	66
Figure 2. 11: PI uptake in SCEP .....	68
Figure 2. 12: Normalized fluorescence intensity changes in calcein AM-staining fast temporal resolution SECP..	70
Figure 2. 13: Normalized fluorescence intensity changes in Thioglo <sup>®</sup> 1 - staining SECP.....	71

## PREFACE

I am very grateful for the help and instruction from my advisor, Prof. Stephen Weber. He is a nice and knowledgeable professor who gave me many useful suggestions on my experimental design and result analysis that inspired me a lot on my research work. He also taught me how to become a creative, independent, wide-open and hard-working chemist, which is very important for my future career.

I thank Prof. Amemiya and Prof. Michael as my committee. Their great knowledge in analytical chemistry gave me a lot of help.

I appreciate the support from all the colleagues in Weber group. They are very kind and cooperative. I obtained many good ideas from them in my research and I am very glad to work with such a good united team.

This work is financially support by NIH R01GM066018.

## **1.0 INTRODUCTION OF SINGLE-CELL ELECTROPORATION**

### **1.1 INTRODUCTION OF ELECTROPORATION**

#### **1.1.1 What is electroporation**

Electroporation, also called electropermeabilization, is a phenomenon that occurs when a high voltage is applied to the cells. In the applied electric field, nanoscale pores form in the cell membrane, thus allowing molecules to be transported into and out of the cells. Pores formation can be reversible or irreversible depending on the electric and cell characteristics. Pores seal in reversible electroporation (RE), while irreversible electroporation (IRE) breaks down the cell membrane permanently and induces death of the cells. Electroporation can lead to several outcomes as shown in Figure 1.1 [1].

Electroporation was first achieved in the late 1960s and early 1970s. People found that the application of high voltage direct current (DC) pulses in  $\mu\text{s}$  and  $\text{kV/cm}$  range to cell suspensions can lead to rupture of the membrane. Later in 1980s and 1990s people found this membrane permeability change could be transient using longer duration (ms scale) and lower

voltage. Currently electroporation has been applied to many cell types including plant cells [2-4], yeasts [5-7], fungi [8-10], bacterial cells [11, 12] and mammalian cells [13, 14].

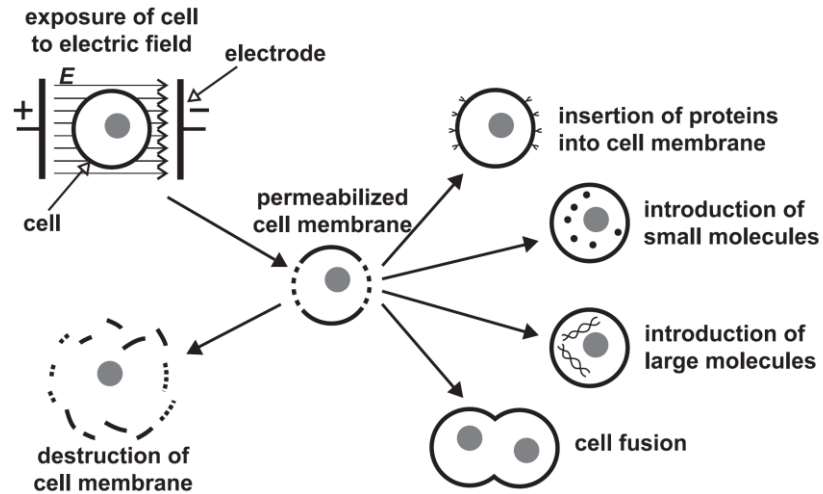


Figure 1. 1: Exposure of a cell to an electric field may result in either permeabilization of cell membrane or its destruction. In this process, the electric field parameters play a key role. If these parameters are within certain range, the permeabilization is reversible; therefore it can be used in applications such as introduction of small or large molecules into the cytoplasm, insertion of proteins into cell membrane or cell fusion. ©2004 Elsevier B.V.

Electroporation is now widely applied in industries and medicine. IRE has been developed in the field of food and environmental industries for microbial inactivation and non-thermal food pasteurization[15]. In terms of RE, electroporative delivery has been carried out both *in vitro* and *in vivo* of many drugs including drugs [13, 14], proteins [16, 17], oligonucleotides [18], RNA [5, 11, 19] and DNA [20]. It is reported that *in vivo* electroporation

may dramatically increase transfection efficiency for a variety of tissues, and consequently led to the rapid development of a new cancer treatment modality called electrochemotherapy [20].

## 1.1.2 Basic electroporation notions

### 1.1.2.1 Transmembrane potential

Though the mechanism of pore formation in electroporation process is still unclear, the following concepts are widely accepted.

When an external electric field is applied to the cell, due to the dielectric cell membrane, a high potential drop arises across the membrane. The potential difference  $\Delta\psi_m$  across a cell membrane consists of two major contributions, natural  $\Delta\psi_0$  (also called as resting potential) and induced  $\Delta\psi_E$  membrane potential differences. In living cell membranes,  $\Delta\psi_0$  is metabolically maintained due to ions concentration gradient. Typically,  $\Delta\psi_0$  is about -40 to -60 mV, where the potential of the outside surface is taken as zero [21].

$$\Delta\psi_m = \Delta\psi_0 + \Delta\psi_E$$

The electrically induced potential difference  $\Delta\psi_E$  is the difference between the potential inside the cell  $\psi_{in}$  and the potential outside the cell  $\psi_{out}$ . In a uniform electric field  $E$ , at a point M on the cell surface at time t  $\Delta\psi_E$  is given by:

$$\Delta\psi_E(t) = \psi_{in} - \psi_{out} = -f g(\lambda) R E \cos\theta(M) (1 - \exp(-t/\tau)) \quad (1)$$

$$\tau = RC_m (r_i + 0.5r_o) \quad (2)$$

where  $\tau$  is the charging time of the pulsed cell membrane,  $f$  is related to the shape of the cell,  $g$  depends on the conductivities  $\lambda$  of the membrane, of the cytoplasm and of the extracellular medium,  $R$  is the radius of the spherical cell (in case the cell is non-spherical, it is replaced by the semiaxis oriented in the field direction [22, 23]),  $E$  the field strength,  $\theta(M)$  the angle between the normal to the membrane at the position  $M$  and the direction of the field (refer to Figure 1.2),  $C_m$  is membrane capacity and  $r_i$  and  $r_o$  are resistivities inside and outside of the cell [24, 25].

The charging time  $\tau$  is typically less than 1  $\mu\text{s}$ , thus the exponential term can be ignored if the pulse length is much longer than a few microseconds. Under the hypotheses that the cell shape is spherical and the membrane is a pure dielectric,  $f = 1.5$  and  $g(\lambda) = 1$  [25].

### **1.1.2.2 Polarization of cells in external electric field**

As stated above, the external electric field induces a position-dependent modulation of the membrane potential difference  $\Delta\psi_E$  which is superimposed on the resting potential difference  $\Delta\psi_0$ . As a result of this spatial distribution of transmembrane potential, cells are polarized under external  $E$ . The anode facing side is hyperpolarized while cathode facing side is depolarized as shown in Figure 1-2. This polarization phenomenon was imaged using potential sensitive fluorescent dye [26].

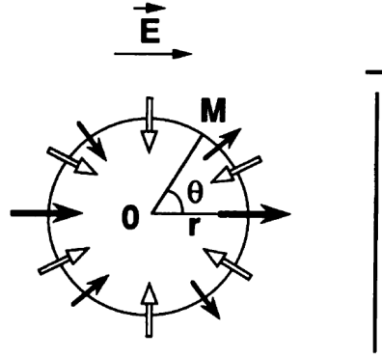


Figure 1. 2: Polarization of a cell in external electric field. The arrows are the vectorial representation of the electrical potential gradient direction. Open arrows for resting potential; closed arrows for electric field induced potential. Their length is indicative of the magnitude of the potential difference[27]. © 1993 by the Biophysical Society

The polarization of cells under external  $E$  causes the anode facing side to become more permeable than the cathode facing side, especially with short pulse duration [28, 29]. This asymmetry of molecular transfer was demonstrated by direct visualization of PI penetration into a single cell [30].

### 1.1.2.3 Critical transmembrane potential ( $TMP_c$ ) for electroporation

It is widely accepted that when  $\Delta\psi_m$  goes above a critical threshold  $\Delta\psi_c$  (or  $TMP_c$ ) electroporation occurs. The critical value has been experimentally determined to be in the range of 200 mV - 1 V. The corresponding critical electric field  $E_p$  ranges from 100 V/cm in terms of large cells such as muscle cells to 1-2 kV/cm in terms of bacteria [27, 31]. It is easy to see that under uniform electric field, larger cell size needs smaller  $E_p$  to reach the critical value (refer to

equation (1) in transmembrane potential part). The critical field  $E_p$  appears to be characteristic quantity of a given cell type, it depends on the cell size and cell species.

#### **1.1.2.4 Kinetic description of reversible electroporation**

Kinetic studies of RE based on experimental monitoring of membrane conductance alteration with submicrosecond imaging [28, 32] led to a description in 5 steps which is widely adopted [25].

##### *(1) Induction*

The external electric field induces an increase in the transmembrane until it reaches the critical value. This step is associated with the threshold  $TMP_c$  of the membrane. A delay may be present due to the charging time  $\tau$  of the pulsed cell membrane. This step is evaluated to be  $< 1 \mu\text{s}$ . Recently the study of nanosecond pulses for electroporation indicates that this step may be as short as several nanoseconds [33, 34].

##### *(2) Expansion*

The induction step is followed by a continuous increase in permeability as long as the field is maintained at an overcritical value [32]. This can be explained by an expansion step. During this stage, the local density of pores increases, and structural reorganization of the membrane presents depending on the pulse duration. The time scale of expansion depends on the pulse duration, typically in the range of  $\mu\text{s} \sim \text{ms}$ .

### *(3) Stabilization*

As soon as the electric intensity decreases to subcritical level, a stabilization process takes place within a few milliseconds. A dramatic recovery of membrane organization occurs, inducing a strongly drop in membrane conductance. Nevertheless, a long living permeability particularly for small molecules persists beyond this step [28].

### *(4) Resealing*

A slow resealing to the membrane intrinsic impermeability then occurs on a scale of seconds and minutes spontaneously. It is a first order process depending on pulse duration, pulse number and ambient temperature [35, 36]. Most of the extent of electroloading takes place during this recovery stage.

### *(5) Memory*

The complete resealing of the membrane prevents the cell from rupture and preserves the viability of cells in most pulsing conditions. Nevertheless, some changes in the membrane properties (flip-flop) and cellular physiological (macropinocytosis) properties remain present on a longer time scale (minutes to hours). The cell alteration may lead to cell death in the long term.

## **1.1.3 Important parameters in electroporation**

Electric field, cellular factors and physicochemical factors all affect the efficiency of electroporation and its applications.

### 1.1.3.1 Electrical parameters

These include pulse amplitude  $E$ , pulse duration  $T_d$ , pulse repetition frequency  $f$ , number of pulses  $N$ , and pulse types (polarity and shape).

(1) *Electric field strength  $E$*

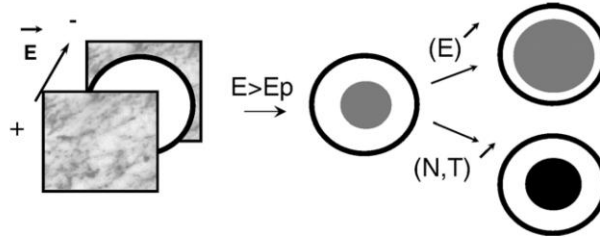


Figure 1. 3: Role of electric field on electroporation. A cell is submitted to an electric field. The gray area represents the cell surface that is prone to be permeabilized. This area increases with  $E$ . When the cell is submitted to a constant  $E$  but to increasing  $N$  and/or  $T_d$ , the size of the potentially permeabilizable area remains constant, but the density of transient permeated structures in that area, i.e., the permeabilization, increases by increasing these parameters (which is represented by gray hatching). © 2006 Elsevier B.V.

As mentioned above, only when  $E > E_p$ , electroporation occurs. For a given  $E > E_p$ , electroporation occurs only inside a cone where  $\Delta\psi_m > TMP_c$ . In a uniform external  $E$ , the half angle  $\theta_p$  of this cone is determined by  $E \cos\theta_p = E_p$ .

Thus  $E$  topologically determines the membrane area at the cell level where permeabilization can occur, while  $T_d$  and  $N$  determine the density and/or size of permeated structures, as shown in Figure 1.3 [31, 35].

Increasing  $E$  may increase the transport of molecules; the tradeoff is that it may induce a loss in cell viability. So researchers seek to optimize pulse durations and other parameters to get best efficiency of electroporability.

*(2) Duration of pulses  $T_d$ , pulse repetition frequency  $f$  and number of pulses  $N$*

The effect of  $T_d$  and  $N$  has been described above. To be specific, prolonged  $T_d$  enhances the transport through the pores but does not increase the pore density, while larger  $N$  can create more pores in the cell membrane [37]. Under conditions where cell viability is preserved,  $T_d$  is shown to be crucial for the penetration of macromolecules into cells. Cumulative effects are observed when repeated pulses are applied. At a constant number of  $NT_d$  duration product, transfer of macromolecules is strongly affected by  $T_d$ . The resealing process appears to be first-order with a decay time linearly related to the pulse duration [35]. There's also a tradeoff, too long  $T_d$  or/and multiple pulses will increase the death rate.

Classical electroporation utilizes pulses in the ms -  $\mu$ s range and electric fields that are near 1 kV/cm. Recently, electroporation of cells has been carried out using very high pulses with a very short duration (3-300 ns, up to 300 KV/cm). Calculations show the transmembrane potential expects to reach 1 V in less than 2 ns. Cellular responses to these previously uninvestigated very short pulse widths are similar to those observed with longer duration pulses. Phospholipids rearrangements and the influx of small molecules from the medium into the cytoplasm has been imaged [33, 34].

### (3) Pulse types

Bipolar waves are reported to have higher efficiency of electropermeability than unipolar waves [38, 39], and significantly reduce the electrolytic contamination caused by the electrode reaction [40]. For different pulse shapes, the duration of above-critical pulse amplitude has a major role in the efficiency of electropermeabilization [41].

Different types of pulse generation techniques are compared by Marko Puc et al. as shown in Table 1-1. A summary of commercial devices can also be found in the same paper.

Table 1. 1: Comparison of most commonly used techniques of signal generation for electroporation [1]. © 2004 Elsevier B.V.

Technique	Advantages	Disadvantages
Discharge of capacitor (exponential decay pulse generators)	<ul style="list-style-type: none"><li>• Simple and inexpensive construction</li></ul>	<ul style="list-style-type: none"><li>• Poor flexibility of parameters</li></ul>
Square wave generator (power transistors)	<ul style="list-style-type: none"><li>• Simple construction</li><li>• Better control of pulse parameters</li></ul>	<ul style="list-style-type: none"><li>• Limitation of output parameters due to semiconductor technology</li></ul>
Square wave generator (pulse transformer)	<ul style="list-style-type: none"><li>• Very safe (possibly to use in clinical environment)</li><li>• Very high pulse amplitudes</li></ul>	<ul style="list-style-type: none"><li>• Limitations of pulse duration and repetition frequency</li><li>• Complex design of pulse transformer</li><li>• Limitation of output current and voltage due to semiconductor technology</li></ul>
Analogue generator of unipolar arbitrary signals	<ul style="list-style-type: none"><li>• Wide flexibility of pulse parameters</li><li>• Arbitrary signal shape</li></ul>	<ul style="list-style-type: none"><li>• Limitation of bandwidth, output current and voltage due to semiconductor technology</li></ul>
Analogue generator of bipolar arbitrary signals	<ul style="list-style-type: none"><li>• Genuine bipolar arbitrary signals</li><li>• Arbitrary signal shape</li></ul>	<ul style="list-style-type: none"><li>• Price</li></ul>
Modular high voltage source	<ul style="list-style-type: none"><li>• High dynamics</li><li>• High currents and voltages</li></ul>	

### 1.1.3.2 Cellular factors

These include cell type, cell size, cell shape, cell density, growth phase and cell cycle.

#### (1) Cell type and cell size

As described above, cell type and cell size are critical for  $TMP_c$ .

### (2) Cell shape and orientation

In equation (1),  $f$  is related to the shape of the cell. Given a uniform electric field, when cell is spherical,  $f = 1.5$ . For prolate spheroids with the long axis perpendicular to the external field,  $1.5 < f < 2$ . For prolate spheroids with the long axis parallel to the external field,  $1 < f < 1.5$ . For oblate spheroids with the short axis parallel to the field,  $f > 2$  [24].

### (3) Cell density

The effect of cell concentration is explained quantitatively by electric field perturbations caused by neighboring cells. Higher cell concentration decreases the local field experienced by a cell, thus affects the efficiency of electroporation and cell survivability [42, 43].

### (4) Cell cycle for eukaryotic cells (Synchronization)

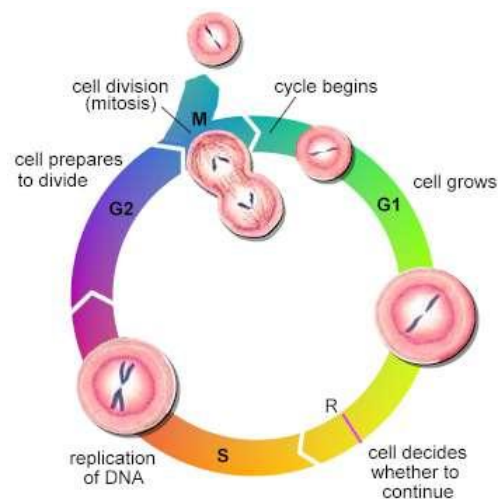


Figure 1. 4: Cell cycle. The cell cycle is divided into four phases: G<sub>1</sub>, S, G<sub>2</sub> and M. Cells in the first cell cycle phase (G<sub>1</sub>) do not always continue through the cycle. Instead they can exit from the cell cycle and enter a resting stage (G<sub>0</sub>). (<http://learninglab.co.uk/headstart/cycle3.htm>)

The cell cycle, or cell-division cycle, is the series of events that take place in a eukaryotic cell leading to its replication. It consists four phases as shown in Figure 1.4. The duration of the cell cycle varies between different cell types. In most mammalian cancer cells it lasts between 10 and 30 hours.

The cell cycle leads to the change of cell state such as size, membrane tension, osmotic pressure and so on, therefore may play an important role in the electroporation process. Nevertheless, few studies of the effect of cell synchronization on cell electroporation have been reported. Sukhorukov et al. reported electric membrane properties of both G1/S phase (arrested by aphidicolin) and G2/M (arrested by doxorubicin) mammalian cells are similar to asynchronous cells [44]. Slight changes of resting membrane potential  $\Delta\psi_0$  during cell cycle have been reported [45]. DNA expression is enhanced in G2/M phase synchronized cells; while synchronization in G1 phase has no effect on permeabilization and transfection [46].

#### *(5) Growth phase*

The study on growth phase effect concentrates on bacterial. Conflicting results about the best electroporation efficiency have been obtained during log phase, lag phase and stationary phase, respectively [47-49].

#### **1.1.3.3 Physicochemical factors**

The composition of the electroporation buffer and ambient temperature also play an important role in electroporation.

### *(1) Electroporation buffer*

The composition of the buffer determines its specific resistivity, osmolarity and  $K^+$ -dependent membrane resting potential, hence influences the electroporation yield [50, 51]. Higher conductivity or/and lower  $K^+$  concentration has been reported to correspond to lower electric threshold [52]. The buffer pH is also important. In general, the buffer composition and pH should mimic the cytoplasm of the cell. The usual intracellular pH is around 7.2. When applying high voltage with long duration, lower salt compositions are usually used to avoid excess Joule heating produced by the high voltage.

### *(2) Temperature*

Ambient temperature has a great effect on electroporation. It acts on electric field, pore resealing and conductivity of buffer. Though conflicting data on the temperature dependence of electrotransfection have been reported, many researchers reported increased susceptibility to permeabilization and a shortened resealing period upon elevated temperature [53-56]. It is reported that cells can be kept permeabilized for up to 4 h at 4 °C, while at 37 °C, the membrane resealing occurs in less than 5 min. A fast resealing at higher temperature increases the viability and hence the transfection efficiency. A higher level of transfection is obtained when Chinese Hamster Ovary cells are pre-pulse incubated at 4 °C and post-pulse incubated at 37 °C [57, 58].

## 1.1.4 Brief introduction to mechanism study of electroporation

### 1.1.4.1 The mechanism of electroporation remains unclear

The actual mechanism of electrically induced instabilities has yet to be well understood. Many theoretical models have been set up attempting to explain the mechanism of electroporation. Some models are concerned with more macroscopic reasons for instability as lipid membrane thinning, related to electrostriction, undulation and elastic properties of the membranes. Other models based on the *Smoluchowski* equation [59-62] find the explanation in formation and expansion of tiny pores. Recently the nanoscale pulse induced electroporation models has stimulated models based on molecular dynamic simulations, which try to explain the pore permeabilization process from the atomic aspect [63-66].

### 1.1.4.2 Pores

#### *(1)Energy barrier*

In spite of the different models for electroporation, there is a common accepted concept about pore creation: the pores form in a scale of nanoseconds, and need to overcome a common energy barrier of  $\approx 45 - 50kT$  [67]. This pore radius-related energy barrier was initially thought as increasing within a critical pore radius  $r_c$  and decreasing beyond  $r_c$  [68], then was later corrected in improved models to be self-constraining (which means the energy barrier keeps increasing with the increasing of pore radius) to prevent resulting uncontrollable pore growth

and expansion. These improved models take into account the feedback brought by the current flowing across the pore on the induced potential difference [69].

(2) *Pore structure*

The only experimental visualization of the actual transient pores was performed by Chang and Reese in 1990 [70]. They used rapid-freezing electron microscopy to examine human red blood cells exposed to a radio-frequency electric field. The observed crater-like pores had a size range of 20-120 nm. Nevertheless, this unique report was criticized as misleading because red blood cells under strong hypo-osmolar conditions were used. As a matter of fact, no such defects were ever observed under iso-osmolar conditions on other cell models [25].

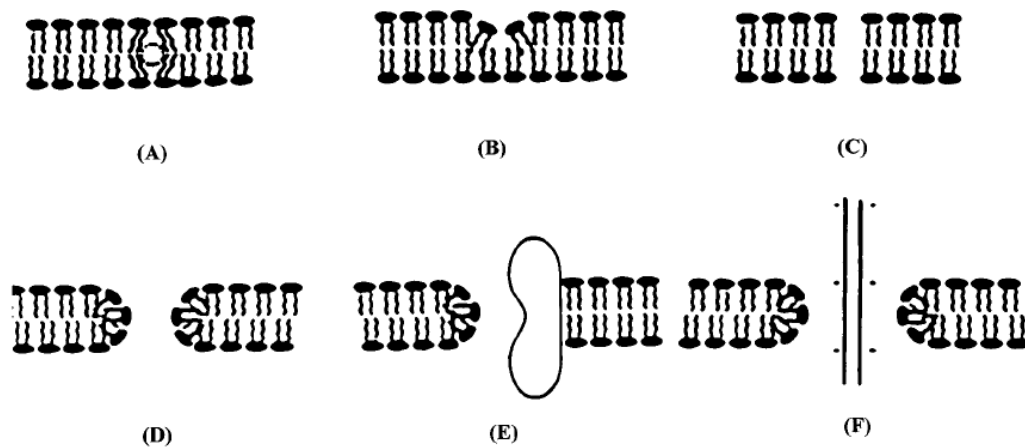


Figure 1. 5: Hypothetical bilayer membrane structural rearrangements. (A) Free volume fluctuation; (B) Local membrane compression and thinning; (C) Hydrophobic pore; (D) Hydrophilic pore; (E) Composite pore involving a

membrane protein; (F) Insertion of a long, charged molecule into a hydrophilic pore while  $\Delta\psi_m$  is large. © 2000 IEEE

Hydrophilic pores are believed to be the major contribution to the transient membrane distortion. It is listed along with other hypothetical bilayer membrane structural rearrangements in Figure 1.5 [71].

### *(3) Models studied pore density, distribution and sizes*

Recent models for electroporation of a single spherical cell in an uniform electric field give theoretical estimation of pore information [59, 72, 73]. According to these models, the pore density can be high in the order of  $10^9$  pores/cm<sup>2</sup>, of which > 97% are small pores having ~1 nm radius. The highest pore density occurs on the depolarized and hyperpolarized poles but the largest pores, which may grow to ~ 0.5  $\mu$ m, are on the border of the electroporated regions of the cell. Despite their much smaller number, large pores comprise 95% of the total pore area and contribute 66% to the increased cell conductance [73].

## **1.2 PROGRESS IN SINGLE-CELL ELECTROPORATION (SCEP)**

### **1.2.1 Why study single-cell electroporation?**

According to the population of target cells, electroporation divides into two groups: bulk cell electroporation and single-cell electroporation (SCEP). It was not until this recent decade that

SCEP has gained attention as a potential approach of single cell handling. Unlike traditional bulk cell electroporation, in SCEP either the single cell is isolated from its population or an inhomogeneous electric field is focused on the target individual cell, leaving neighboring cells unaffected. SCEP is a powerful tool for single-cell manipulation and analysis, it helps to gain knowledge of cells on a micro-basis of one individual cell, which is very important in understanding the cytophysiological process inside a single cell, how/why the individual differs from each other, how one affects the whole and *vice versa*. These could also be incredibly useful for applications such as converting single cells into intracellular biosensors and administering genes or drugs into single cells in complex tissues such as the brain [74].

Because of the complex system condition in SCEP, which especially comes from the non-uniform electric field of microtechnology, it is hard to set up a theoretical model for calculation. So far most researchers focus on the technique development of SCEP and the reported experimental results have been mainly qualitative.

### **1.2.2 SCEP with solid microelectrodes**

SCEP with subcellular spatial resolution, high transfection efficiency and survival rate was first accomplished with solid microelectrodes [75]. Microelectrodes are flexible in usage and low voltage (several volts) is enough for electroporation.

The microelectrodes for SCEP have mainly been developed by Dr. Owe Orwar's group. In 1998 they first performed SCEP [75]. Carbon fiber microelectrodes with tip size of  $\approx 5 \mu\text{m}$

in diameter were placed 2-5  $\mu\text{m}$  away from adherent cells at an angle of 0–20° and 160–180° with respect to the object plane as shown in Figure 1.6(A). A single 1 ms rectangular low voltage pulse ( $\sim 2$  V) electroporated cells with 97% transfection yield and survival rate. Later this microelectrode technology was combined with patch clamp glass pipette positioned in 90° angle to the electrodes to record the current across the buffer (membrane) and give  $TMP_c$ , pore expansion and resealing information (Figure 1.6 (B)) [76]. In 2001 they substituted the patch clamp pipette with a microinjection pipette to expose the cell to high concentration of analytes during electroporation, which showed a success transfection rate of  $34 \pm 7\%$  [77].

Despite the above success in SCEP, the solid microelectrode method has many disadvantages: (1) loading agents need to be added to the buffer solution surrounding the cell or delivered specifically to the targeted area by using, e.g., a superfusion micropipette; (2) Potential loss must be taken into account at the electrode/solution interface due to electrode reaction and formation of double layer; (3) Some potential cytotoxic products such as oxides are produced at the electrode, especially when long pulse durations and short cell-electrode distances are applied. To overcome these problems, people are looking for other SCEP methods.

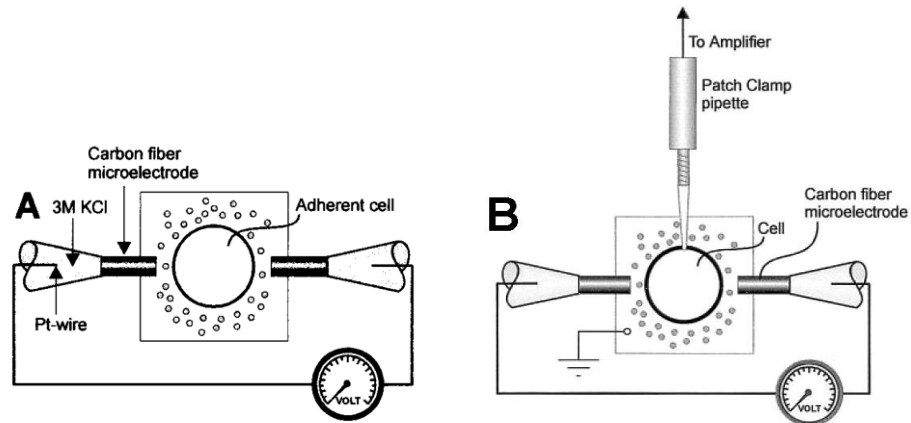


Figure 1. 6: (A) SCEP with two carbon fiber microelectrodes; (B) Combining with patch clamp technique. © 2000 by the Biophysical Society

### 1.2.3 SCEP with patch micropipette and capillaries

Many researchers have shown interests in SCEP with micropipette and capillaries because of their advantages over microelectrodes system: (1) they can delivery cell-loading agents through the micropipette/capillaries by electroosmotic and electrophoretic flow; (2) Electrode reactions take place far away from the electroporated cell, thus dramatically decrease the toxic product problem.

#### 1.2.3.1 Micropipet

The electrode close to the cell is a solute-filled micropipette made of filament fused glass with a metal electrode inside. Another electrode couples with this micropipet electrode to carry current through the target cells. Usually the micropipette is pushed against the cells to create

membrane tension that lower the required voltage, and the volume of inserted molecules can be as small as the micropipet tip ( $< 1.0 \mu\text{L}$ ).

The micropipet system was first developed by Karlsson et al. in 2000 [78]. They combined micropipet electroporation with pressure-driven microinjection for efficient loading of biopolymers and colloidal particles into single-cell-sized unilamellar liposomes. As shown in Figure 1.7, single liposomes were positioned between a  $\sim 2 \mu\text{m}$  tip diameter solute-filled glass micropipet containing a Pt electrode and a  $5 \mu\text{m}$  diameter carbon fiber electrode. The induced dielectric membrane breakdown facilitated the penetration of micropipet tip into the liposome to inject a small volume of loading agents.

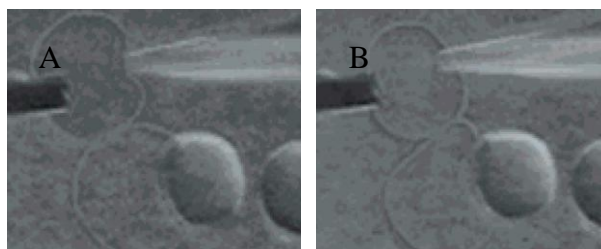


Figure 1. 7: Electroinjection of fluorescein into a giant unilamellar vesicle with a microelectrode and injection micropipette. (A) A mechanical pressure was applied on the vesicle by moving the injection tip toward the microelectrode, forcing the vesicle into a kidneylike shape. (B) By applying a voltage pulse, the membrane was permeabilized, the vesicle slid onto the injection tip, and a fluorescein solution was injected into the vesicle. © 2000 American Chemical Society

In 2001 Haas, Sin et al. performed a delivery of DNA or other macromolecules into single neuron and glia in the brain of intact *Xenopus* tadpoles or rat hippocampal slices merely by SCEP using micropipet method [79]. Figure 1.8 shows the setup. A silver wire placed inside the filament micropipette having a tip diameter of 0.6–1  $\mu\text{m}$  filled with loading solution was connected to a silver electrode in the circuit. A voltage of 10-80 V was used. Optimization of electric parameters led to a transfection efficiency of 20% in vivo [80].

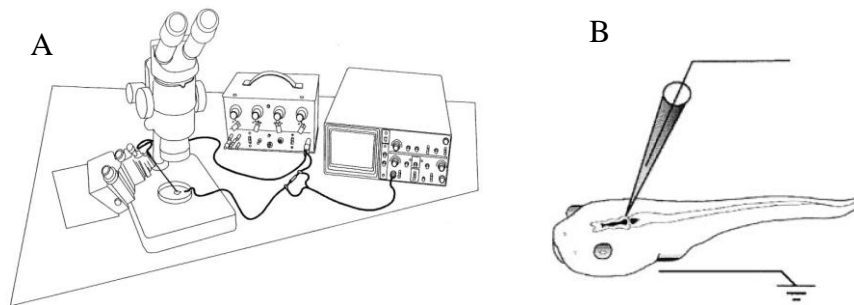


Figure 1. 8: SCEP of slices with micropipette. (A) The SCEP setup. The current passing through this circuit can be monitored by measuring the voltage drop across a known resistor with an oscilloscope. (B) SCEP of neurons in vivo was carried out by inserting a glass micropipette filled with DNA solution into the tadpole brain. Stimulation delivered between the micropipette and an external ground electroperated a single cell at the micropipette tip. © 2001 by Cell Press

The low permeabilization efficiency was improved by accurate positioning of micropipet contacting the cells. To do this, Rae applied modified patch-clamp techniques [81]. A cultured cell was indented by a micropipet having a pulled tip  $\sim 0.5 \mu\text{m}$  and electroperated

through the same micropipet when the resistance increased by 25% due to the indentation. A success rate of 60–100% was obtained using 5~10 V square pulses for gene insertion. Rathenberg used two-photon microscopy for real-time visualization at the cellular level when electroporating single cells in neurons using fluorescently labeled oligonucleotides and plasmid DNA ( figure 1.9), which led to a high efficiency of 50%~80% [82].

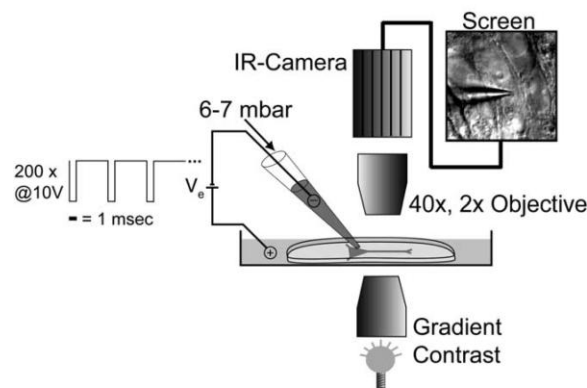


Figure 1. 9: Illustration of the modified SCEP-mediated transfection setup. The culture was placed in a perfusion chamber and visualized using gradient-contrast illumination and IR video microscopy. Individual neurons can be identified on the monitor screen. The DNA filled micropipette can be targeted precisely to the membrane of a single soma. © 2003 Elsevier B.V.

SCEP using micropipet has been widely used. To increase the throughput, in 2006, Bae automated SCEP using the modified patch micropipet method [83]. Many applications have been reported concerning morphological staining, DNA and macromolecules transfection, investigation of  $Ca^{2+}$  physiological role, electrophysiological response after pulse and so on [84-88]. Typically people use small micropipet tip with a diameter of  $0.5 \mu m \sim 2 \mu m$  for SCEP

with micropipet, which is also the standard size for patch-clamp recording. Nevertheless, larger tip opening is also used with stronger voltage pulses. Uesaka used a tip diameter of 30-50  $\mu\text{m}$  and 200-300  $\mu\text{m}$  for in vitro morphological and electrophysiological study of neurons [89, 90].

### **1.2.3.2 Electrolyte-filled capillaries (EFC)**

Fused-silica capillaries filled with electrolyte are also favorable for SCEP. The main differences between EFC and micropipet are that (1) EFC contains no electrode or filament fused in the wall and thus current goes through electrolyte inside the EFC; (2) EFC is placed away from target cells at a distance of several microns. Similar to micropipet method, EFC minimizes volume of loading solute, can obtain high spatial resolution with reduced physical dimension. Less cell trauma is expected because there is no physical force added to cell membrane by the tip, and the electrode is farther from the cell. The EFC is also used for separation in capillary electrophoresis (CE). Electroporation and chemical fractionation might be performed with the same EFC. The disadvantage is that longer pulse duration and higher voltage are required because of high resistance inside EFC.

Figure 1.10 shows a typical experimental setup of SCEP using EFC built by the Orwar group [91]. An EFC (30 cm long, 375  $\mu\text{m}$  in outer diameter, 30  $\mu\text{m}$  in inner diameter) with outlet end tapered to outer diameter  $\sim 50 \mu\text{m}$  was placed 5  $\mu\text{m}$  away from the cells. A large-voltage pulse (2 kV-10 kV, duration 5 s) applied across the EFC gave rise to a small electric field outside the terminus of the EFC, which caused pore formation in cell membranes. The electroosmotic flow delivered agents at the site of pore formation. The electroporation protocol

was demonstrated by introduction of fluorogenic dyes into single NG108-15 cells and small populations of cells in organotypic hippocampal cultures *in vitro*, and more testing on rats brain *in vivo*. Patch-clamp recordings were performed in the whole cell and cell-attached configuration. The electroporation region had diameters of 50-100  $\mu\text{m}$ . They also used untapered capillaries with the same size for electroporation of single targeted cell or small confined groups with higher voltage and longer duration (DC 10 kV, duration 5-60 s, cell-capillary gap distance 20-40  $\mu\text{m}$ ) [92], and even broader capillaries (0.4 mm inner diameter) but lower voltage and shorter duration (gap height 50-100  $\mu\text{m}$ , 200-225 V pulses of 10-25 ms) for scanning electroporation [93].

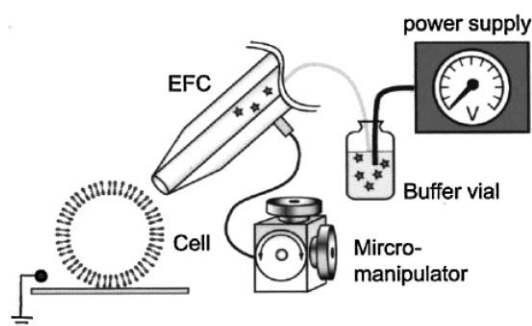


Figure 1. 10: SCEP with EFC: schematic picture of the experimental setup. © 2001 American Chemical Society

When inner diameter of the capillary is uniform, current density and electric field  $E$  are all uniform inside the capillary.  $E$  is approximated as  $\psi/L_c$  where  $\psi$  is the applied potential in volts and  $L_c$  is the length of the EFC. The major potential drop occurs inside the capillary. Then

the magnitude of the electric field decays quickly along the axis of symmetry of the EFC lumen extending out into solution, which is given by:

$$E(Z, \Psi) = \frac{\Psi}{L_c} \left[ \frac{Z}{[1 + (Z)^2]^{1/2}} - 1 \right]$$

where  $Z$  is the dimensionless distance from the EFC tip,  $z/a$ , where  $z$  is the distance from the EFC tip and  $a$  is the EFC lumen radius [91].

SCEP with EFC is also studied in our lab. Instead of using a uniform inner diameter capillary, we use a pulled tip fused-silica capillary with tip opening  $2 \sim 5 \mu\text{m}$  to obtain a much higher spatial resolution. This micro-scale tip gives more complicated electric field distribution. Most potential drop occurs at capillary tip, and decays quickly when extending into solution outside EFC. I will describe SCEP using the pulled EFC later in this chapter.

#### **1.2.4 SCEP with microfabricated chips**

A fast growing part of SCEP is the employment of microchips. Microchips have many merits: (1) Integration with separation and detection and single-cell analysis thereof, (2) small sample amount, (3) high surface/volume ratio decreases heat effect, (4) automated SCEP can be easily developed with high efficiency and throughput, and (5) selectively trapping of specific target cells (for instance, via antibody-antigen reaction). The disadvantages are that fabrication is time-consuming with high-cost, and in most cases it can only use fixed microelectrode.

In 1999 the Rubinsky group first developed the SCEP microchip. Using standard silicon microfabrication technology they built a vertically stacked device with two microfabricated

silicon substrates bonded together with a glass cover slip [94, 95]. A microhole etching through the nitride membrane connected the fluid chambers and electroporation electrodes, producing a constricted field as illustrated in Figure 1.11 (A). A single cell was flowing-through, captured in the microhole by pressure difference, electroporated by the constricted field, uploaded with exogenous compounds, released and replaced by the next cell. Current measurement flowing between the electrodes gave the information of cell trapping and electroporation status as well as the breakdown voltage. Later their group presented a new microchip coupling microfluidic channels enabling cell manipulation and thus SCEP in a flow-through manner. Membrane impermeable nucleic acid stain YOYO-1 and enhanced green fluorescent protein (EGFP) were loaded into ND-1 cells with a 100% gene transfer rate under controlled electroporation (Figure 1.11 (B)). Further studies showed that nanoscale channels formed between exterior of the cell and pore wall, which may need consideration when performing micropore electroporation [96]. Similar SCEP setup based on PDMS was successfully developed by Kurosawa in 2006 at a yield of almost 100% with 1.5 V pulses regardless of the cell size, shape or orientation [97]. Instead of using microholes of 1-3  $\mu\text{m}$ , Sarkar applied a flow-through microfabricated 40- $\mu\text{m}$  sense-porate aperture to electroporate the cells. Cells can pass the aperture and be identified by impedance change [98].

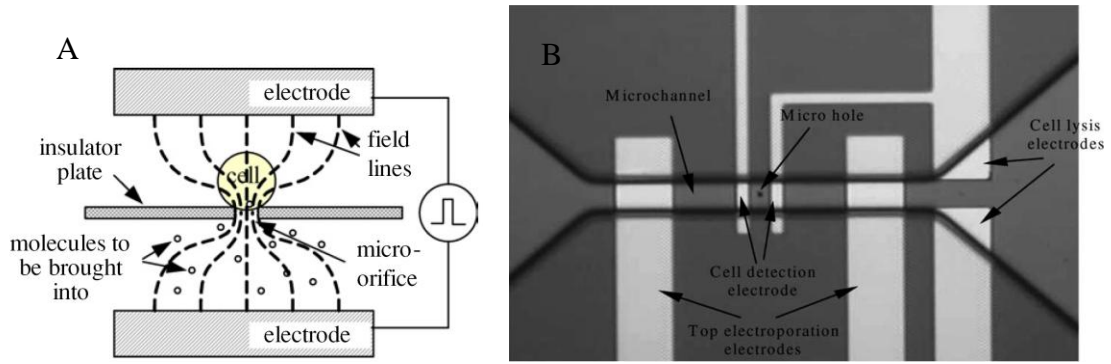


Figure 1. 11: First SCEP microchip. (A) Electroporation using the field constriction [97]. © 2006 IOP Publishing Ltd; (B) Optical image of the layout of microhole, microchannel and integrated electrodes of a flow-through microelectroporation chip with microfluidic channels for precise cell transport. © 2003 Elsevier Science B.V.

In 2005, Luke Lee group developed a PDMS microfluidic chip that can laterally immobilize and locally electroporate cells in parallel (Figure 1.12) [99, 100]. The electrode was not incorporated on chip, eliminating production of adverse products from electrode reactions. Potential drop occurred mainly in the trapped cell membrane area. HeLa cells were electroporated using low voltages ( $\sim 0.76\text{V}$ ) with escape of Calcein and entrance of Trypan blue. Cells were trapped by negative pressure via an attached syringe. This integrated multiple patch-clamp array microfluidic PDMS chip was recently mated with disposable bottom-less 96-well plate, enabling cells to be manipulated and monitored individually [101]. Usage of Ag/AgCl electrodes and a patch clamp amplifier allowed accurate current traces and therefore cell resistance variation monitoring.

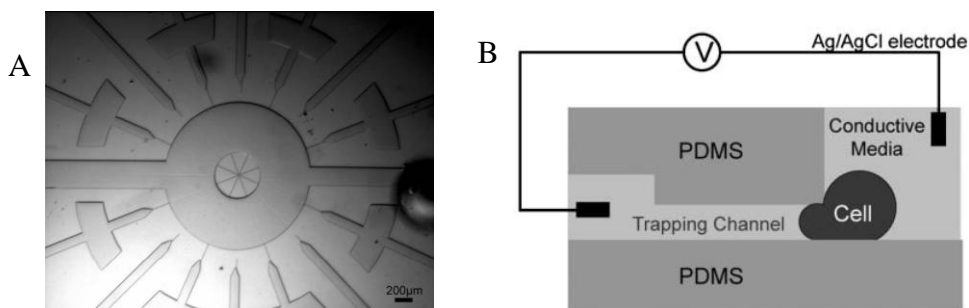


Figure 1. 12: Layout of the chip and cell. (A) A multiplexed patch clamp array for high-throughput measurements. (B) A schematic view of the cross-section of the chip. ©The Royal Society of Chemistry 2005

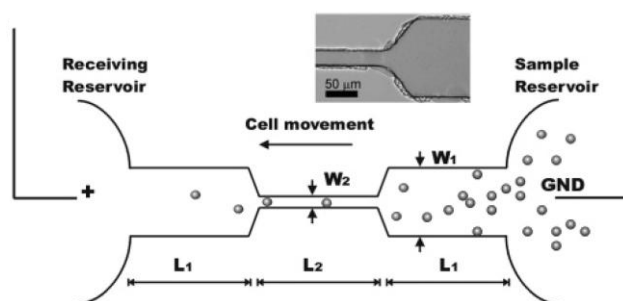


Figure 1. 13: Schematic view of the electroporation device. Cells in the sample reservoir flowed to the receiving reservoir in a DC field. Electroporation was confined in the narrow section of the channel due to the amplified field inside. The inset shows a microscope image of a part of a fabricated device. The devices have the following dimensions:  $L_1$  2.5 mm,  $L_2$  2.0 mm,  $W_1$  213 μm and  $W_2$  33 μm. © 2006 American Chemical Society

In 2006 Wang reported a simple technique for SCEP with high throughput on a microfluidic platform (Figure 1.13) [102, 103]. Electroporation only happened in a defined section of a microfluidic channel due to the local field amplification by geometric variation.

Exposure time of the cells to this high field was determined by velocity of the cells and length of the section. Chinese hamster ovary cells were electroporated reversibly and irreversibly by attenuating field strength. The correlation between cell swelling during electroporation and buffer osmolarity was also studied.

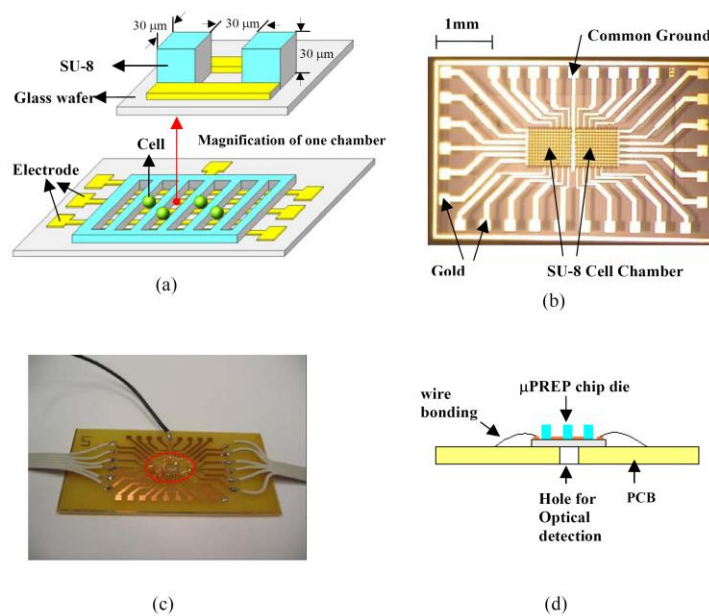


Figure 1. 14:  $\mu$ PREP chip. (a) 3D schematic diagram of the  $\mu$ PREP chip, (b) a  $\mu$ PREP chip die. The electrodes in vertical direction were used for multiple electric field input, while those in lateral direction were for future current detection during electroporation, (c) Photograph of a packaged device. Within the red circle is the  $\mu$ PREP chip die which was wire-bonded on the PCB board, (d) Schematic diagram of a packaged device for optical detection. © 2005 Elsevier Science B.V.

He et al. brought up a new micro pulsed radio frequency electroporation ( $\mu$ PREP) chip based on MEMS technology illustrated in Figure 1.14 [104, 105]. A large amount of cells can be electroporated under different pulse conditions at the same time. A statistical “phase diagram” resulting from parametric study (pulse amplitude and pulse duration vs. fluorescent intensity variations and cell viability) helped to optimize electroporation efficiency and cell viability as shown in Figure 1.15 (A). More recently they modified the chip with increased height electrodes ( from 0.5  $\mu\text{m}$  to 12  $\mu\text{m}$ ) to increase permeabilization efficiency of the cells at a more powerful 3D electric field [106]. Electroporation phase diagram of Hela cells from loading of five different size fluorescence-labeled dextrans (from 10 kDa to 70 kDa with approximate physical diameters of 4.6 nm to 12 nm) showed a strong dependence between permeability and molecular weight, and a size cut-off criterion of  $\sim 40$  kDa (Figure 1.15 (B) ).

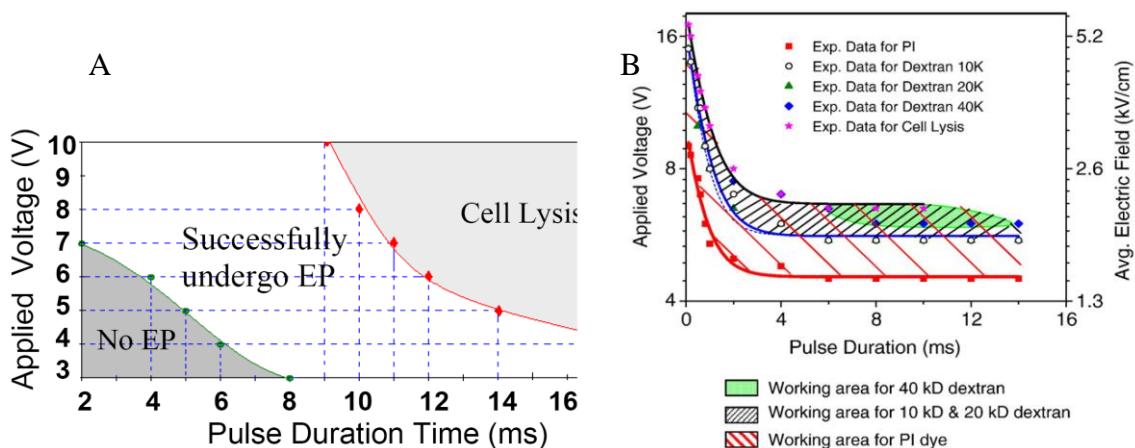


Figure 1. 15: The phase diagram for electroporation and cell lysis. (A) PI uptake in cabbage cells, (B) electroporation of Hela cells with four different sizes of dextrans. © Elsevier B.V.

### 1.2.5 Other techniques for SCEP: multi-walled carbon nanotubes

In 2005 Rojas-Chapana reported a plasmid delivery system based on water dispersible multi-walled carbon nanotubes (CNTs) that can simultaneously target the bacterial surface and deliver plasmids into the cells via temporary nanochannels across the cell envelope [107]. No electrodes were needed. Water dispersible CNTs (~40 nm in diameter, <0.6  $\mu\text{m}$  in length) having an anionic surface charge attached to the surface of Gram negative bacteria mainly by an electrostatic interaction between the CNTs and the likewise charged bacterial surface. On the other hand, the effect of a microwave electromagnetic field pulse on the interaction of CNTs with the cells led to electroporation through individual CNTs. Using this technique, gold nanoparticles were transported into *E. coli* cells without affecting cell growth and cell morphology ( Figure 1.16).

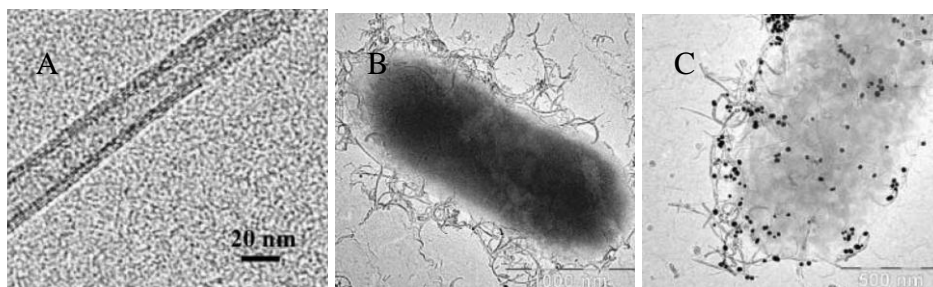


Figure 1. 16: TEM image of CNT electroporation. (A) an individual CNT, (B) bacterial cell interacting with CNTs, (C) bacterial cell interacting with CNTs and gold nanoparticles by microwave-treatment. ©The Royal Society of Chemistry 2005

### 1.2.6 Single-cell analysis and SCEP

A prominent potential application of SCEP is to do single-cell analysis without affecting natural behavior of the target cells. Electroporation is considered as an appropriate technique being able to keep the proliferation and viability of cells. It not only provides a way to introduce interest molecular probes into a single cell and prohibit alterations in cell contents due to the loss of cell functions, but also makes it possible to have a dynamic study in a long time at the single or subcellular level. On the other hand, analysis based on single cell is an essential part during the study of SCEP.

Single-cell analysis has become the focus of the frontier with great challenge in analytical chemistry [108]. It is the pith of biological reductionism. Thousands of different biochemical processes are simultaneously performed with the aid of proteins and information stored in DNA. Multiple processes interact, giving rise to complicated biological phenomena. Due to the ultra small size of single cell (diameter 7-200  $\mu\text{m}$ , volume fL-nL), ultratrace amount of components (zmol-fmol) and ultrarapid biochemical reactions (ms), single-cell analysis typically requires high sensitivity, high selectivity, high temporal resolution and ultrasmall sampling-volume.

A conventional procedure for single-cell analysis is: cell manipulation (by dielectrophoretic tweezers, optical tweezers, micropipets and microfluidic chips)  $\rightarrow$  injection (into channels of capillary or chips)  $\rightarrow$  lysis (by detergent, hypoosmotic solution, ultrasonication, laser pulse and electric pulse)  $\rightarrow$  separation and detection (CE or flow

cytometry with laser-induced fluorescence (LIF) electrochemical detection and mass spectrometry) [109]. Hua reported a single-cell analysis combining electroporation for intracellular immuno-reaction followed by CE-LIF detection in this typical procedure [110].

A variety of microscopic techniques have been developed for imaging analysis of single cells including a common fluorescence microscope/or an inverted epifluorescence microscope equipped with a charged coupled device (CCD) camera, confocal laser-scanning microscopy (CLSM), multiphoton fluorescence microscopy, total internal reflection fluorescence microscopy (TIRFM), atomic force microscopy (AFM), and scanning electrochemistry microscopy (SECM) etc.

Studies on dynamic process of single-cell are very important for understanding its function and activity. Novel analysis techniques with high spatial and time resolution have been developed for real-time dynamic monitoring of the signal molecules released from single living cell, or even from subcellular vesicles. Combination of ultra-microelectrodes with a patch clamp has been used for the real-time measurement [111]. Techniques such as laser ablation, chemical etching and lithography have been used to fabricate vials with volumes in the nanoliter or even picoliter range. These micro-machined ultra-small-volume vials have been used for sample preparation and detection [112].

As described in SCEP techniques, the advanced techniques of single-cell analysis help to understand the cell behavior under electroporation by fluorescence imaging. One challenge for application of SCEP in single-cell analysis is the collection and analysis of the leaking

substances from a single living cell while electroporating it. However, it is believed that SCEP will ultimately be a protocol for real-time, single living cell analysis.

### **1.2.7 Optimization of SCEP for high efficiency and survivability**

As mentioned before, so far most reports of SCEP are qualitative. Researchers find optimized pulse conditions to obtain high efficiency RE for their specific setup, but no other variables have been investigated in detail. In the following text, I will describe what variables affect the results of SCEP and some latest progress achieved in study with EFC. Then a possible way for technique improvement will be proposed leading to our efforts in the recent and future work.

#### **1.2.7.1 Larger variance in SCEP than in bulk electroporation**

Different from bulk electroporation where the average information is collected and uniform electric field is applied, SCEP is characterized by results from individual cells and a restricted non-uniform electric field in most cases. Small alterations in the device geometry and individual cell conditions matter more than in bulk electroporation and would induce a lot variance. Thus a large variance is expected for SCEP. This is demonstrated in our experiments with EFC where the same EFC, same geometry (tip-cell distance) and same pulse conditions are applied on two cells with similar shape and diameter in the same cell dish (Figure 1.17).

Statistical analysis is necessary in SCEP to reveal the origins of the variance and optimize parameters for best efficiency and survivability, like the phase diagram described by He [106]. In the other way, efforts should be paid to narrow the variance, which in the other

words is to get better control of the SCEP by governing the variables. This is one aim of our experimental work.

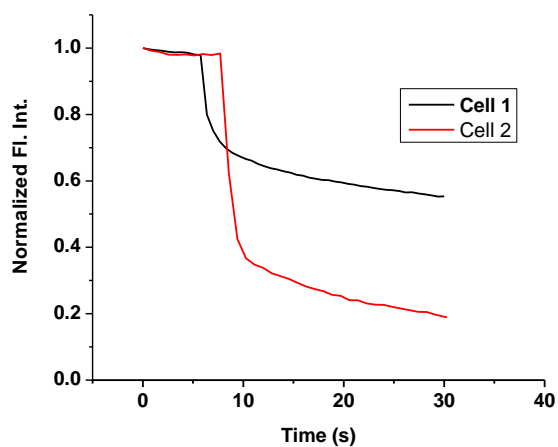


Figure 1. 17: Whole-cell fluorescence intensity vs. time during electroporation of single A549 cells. Cells were pre-stained by Thioglo<sup>®</sup> 1. Upon electroporation, the fluorescent Thioglo<sup>®</sup> 1-GSH complex flew out of the cell, resulting the decrease of whole-cell fluorescence intensity. The data were normalized by setting the initial fluorescence intensity as 1.

### 1.2.7.2 Distance is a vital factor for electric field distribution

As a matter of fact, all the parameters (electric parameters, cellular factors and physicochemical factors) discussed in chapter 1.1.3 act on SCEP. In this miniaturized electroporation environment, the geometry effect on electroporation is magnified. One most important factor among them is the distance (or position) of microelectrodes or micropipette or EFC with respect to the target cells.

In our group, pulled EFC are used for SCEP to achieve high spatial resolution. Earlier statistical analysis based on experimental results with an pulled EFC demonstrated that the distance between the cell and capillary tips greatly affects electroporation efficiency and cell survivability in a degree over the pulse duration, cell size and cell shape [113, 114]. This is because the strength and distribution of the inhomogeneous electric field dramatically relies on tip-cell distance, as reported by numerical simulation using a finite element method (FEM) program Comsol Multiphysics [113]. The strong relationship between potential drop and distance was also examined in the case of microelectrodes and being considered for electroporation device optimization [106, 115].

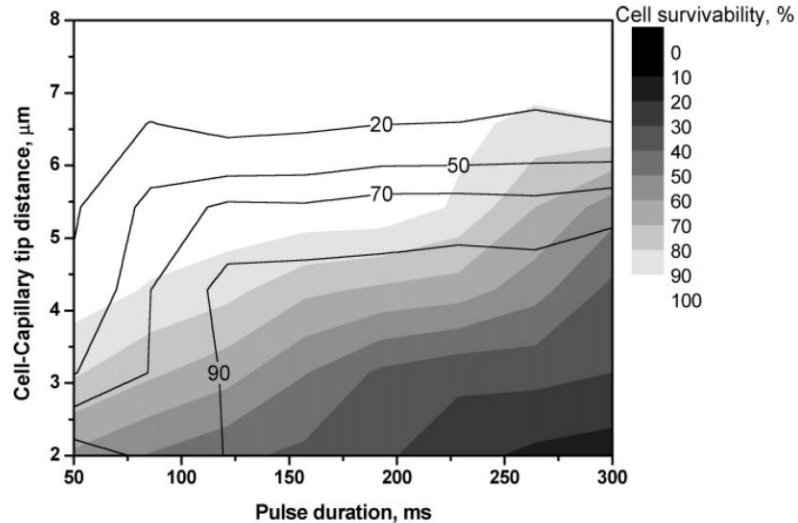


Figure 1. 18: Determination of optimal parameters to achieve maximum cell survivability and electroporation. Contour plot of the fraction of electroporated cells (solid contour lines) superimposed on a contour plot of cell survivability (shaded contour). The contour plot of cell

survivability percentage was plotted as a function of the pulse duration and cell-capillary tip distance. © 2007 American Chemical Society

In the next experiments chapter, I will explain how the electric field looks like at the tip of a pulled capillary when extending into solutions by simulation. When the pulse generators limit the pulses strength and duration, adjusting the capillary geometry and the tip-cell distance is an effective complementary method to yield best electroporation. A vivid example in Figure 1.18 came from our previous work by maximizing the cell permeabilization and viability simultaneously using a 5  $\mu\text{m}$  opening EFC.

Smaller tips usually lead to more dependence of electroporation yield on the cell-tip distance. Thus precise manipulation of distance is required to get good control of electroporation. The positions of microelectrodes in microchip have always been fixed. While in the cases of using EFC or solid electrodes, micromanipulators are applied. I have tried to set up electronics for accurate distance control. Details will be described in the experimental chapter.

### **1.2.7.3 Small-sized cell is a challenge**

Our previous research reveals that small-sized cells require severer condition for electroportion than large cells, which is consistent with the electroporation theory. However, the results also shows that small cells tend to die after being electroporated. The contour plots in Figure 1.19 indicate that when using a 5  $\mu\text{m}$  opening capillary, a wide range of values of pulse duration and

cell-capillary tip distance can give good results for a large spherical cell (plot C); while small cells have a small probability for simultaneous cell survivability and success [113]. Electroporation in a milder extracellular HEPES buffer where we find fast resealing happens gives the similar results (data not shown).

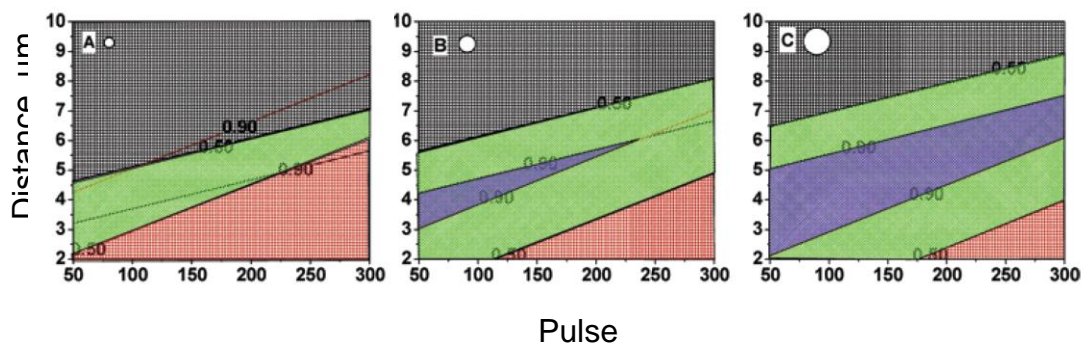


Figure 1. 19: Contour plots of probabilities of cell survivability and electroporation success as a function of pulse duration and cell-capillary tip distance and cell properties. Cell diameters: (A) small (19  $\mu\text{m}$ ), (B) median (25  $\mu\text{m}$ ), and (C) large (39  $\mu\text{m}$ ). Black area: 0-50% electroporation success. Red area: 0-50% cell survivability. Green area: >50% electroporation success and >50% cell survivability. Blue area: >90% electroporation success and >90% cell survivability.

© 2007 American Chemical Society

#### 1.2.7.4 Our hypothesis of cell electroporation and survivability

Two dimensional simulation (details provided in the experimental section) of above different size cells gives the electroporated membrane area (PoreArea), fraction of electroporated membrane area (FEA) and the maximum TMP (at  $\theta = 0$ ). The capillary in these simulation has

a total length of 15 cm, inner diameter (i.d.) of 100  $\mu\text{m}$  and outer diameter (o.d.) of 375  $\mu\text{m}$ , its end close to the cell being pulled to form a tip with a taper length of  $\sim 2\text{mm}$  and i.d. = o.d. = 3.6  $\mu\text{m}$ . Figure 1.20 shows that given the same tip-cell distance, smaller cells have smaller electroperated areas but larger FEA and smaller maximum TMP. Further 3D simulation shows similar trends.

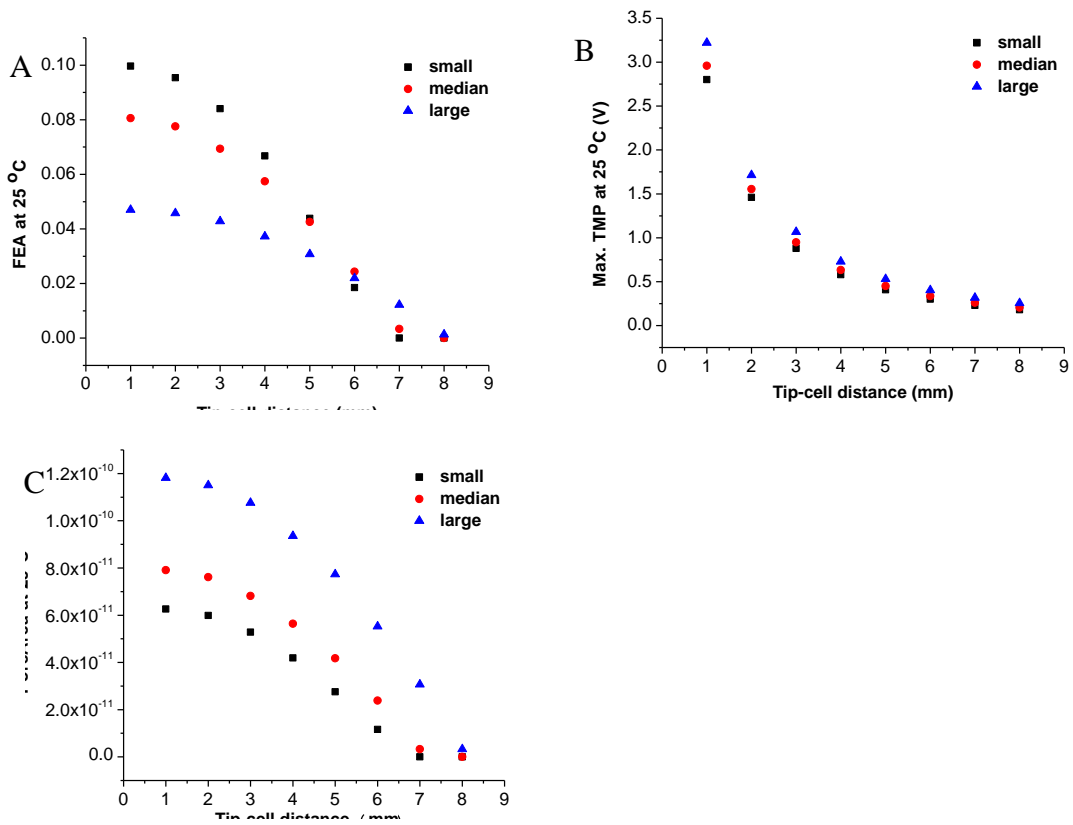


Figure 1. 20: Simulated FEA, Maximum TMP and electroperated area plotted as a function of distance for different sized cells. Cell diameters: small (19  $\mu\text{m}$ ), median (25  $\mu\text{m}$ ), and large (39  $\mu\text{m}$ ). Tip size: 3.6  $\mu\text{m}$ . A 500 V square DC pulse is applied.

It is easy to link maximum TMP with the probability of electropermeabilization according to the existence of TMP threshold. Therefore, a rational conclusion from both the simulation and transmembrane potential theory (refer to equation (1)) is that smaller maximum TMP can cause small cells harder to be electroporated than large cells. An additional important point about the influence of TMP is that too large TMP will induce membrane breakdown.

In the meanwhile, it seems that the large FEA might be the cause of death of small cells. It is of great possibility because large FEA means large extent of intra-extra cellular substances exchange, which is an origin of cell death during electroporation.

To summarize, based on the present theory, simulation and experimental results, we hypothesize that large maximum TMP means high probability of electroporation while small FEA leads to high cell survivability. Following this hypothesis, we seek for appropriate solution to electroporate small cells with simultaneous maximization of electroporation efficiency and survivability.

## **2.0 SCEP WITH EFC MICRO-TIPS**

### **- INSTRUMENTATION, EXPERIMENTS AND SIMULATION**

#### **2.1 INTRODUCTION: SMALLER TIP SIZE OF EFC MAY SOLVE THE PROBLEM OF SMALL-SIZED CELLS**

Through simulation, we find small capillary tips give small FEA at the same maximum TMP as shown in Figure 2.1. A clearer comparison for a 2  $\mu\text{m}$  tip and a 3.6 $\mu\text{m}$  tip with regard to the relationship of FEA and maximum TMP is given in Figure 2.2. As we hypothesize, the smaller tips should benefit electroporation of small cells while keeping the same viability.

Therefore one of our aims is to use small tips ( $\sim 2 \mu\text{m}$ ) for SCEP to improve the probability of electroporating small cells reversibly. It is a challenge in some extent because of increased technical difficulty when handling small tips, and enhanced demand for accurate control of the distance between capillary tip and the cell.

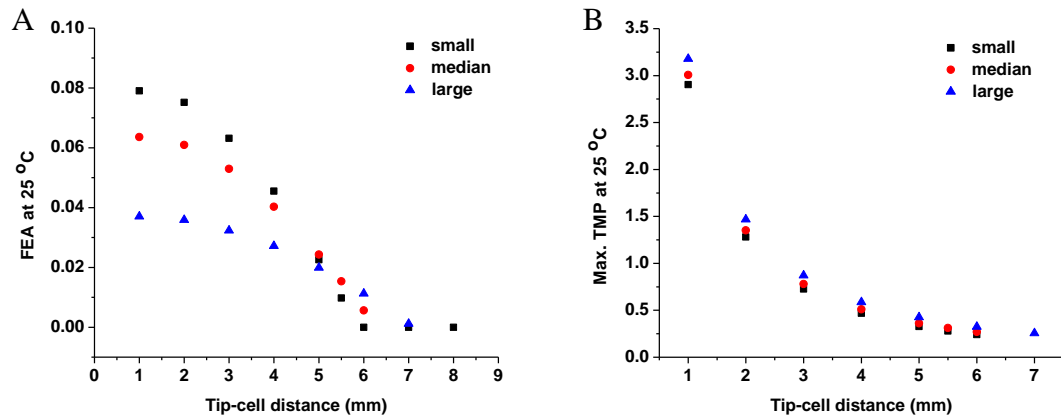


Figure 2. 1: FEA and Maximum TMP plotted as a function of distance for different sized cells at 25 °C. Cell diameters: small (19 μm), median (25 μm), and large (39 μm). Tip size: 2 μm.

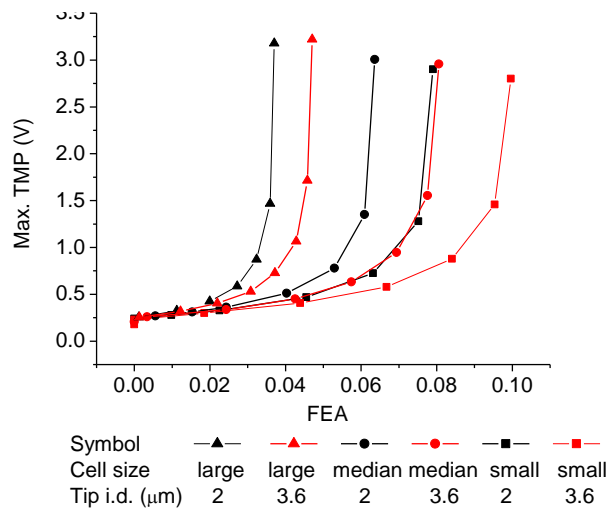


Figure 2. 2: Comparison of 2 μm and 3.6 μm tips regarding FEA and maximum TMP for different sized cells at 25 °C. At the same FEA, smaller tip results larger maximum TMP.

## **2.2 MATERIALS AND METHODS**

### **2.2.1 Materials**

The chemicals used for buffer preparations were all of analytical grade and purchased from Sigma (St. Louis, MO). Thioglo-1 was purchased from Covalent Associates (Woburn, MA). Propidium iodide, calcein AM and NeutrAdivin FluoreSphere were purchased from Invitrogen/Molecular Probes (Eugene, OR). A549 cell lines were obtained from American Type Culture Association (Manassas, VA). Basal medium Eagle (BME), 0.25% trypsin-EDTA, One Shot™ fetal bovine serum (FBS), L-glutamine, and penicillin- Streptomycin were all obtained from Invitrogen, GIBCO (Carlsbad, CA). Milli-Q (Millipore Synthesis A10, Billerica, MA) water was used. Extracellular buffer consisted of NaCl (140 mM), KCl (5 mM), MgCl<sub>2</sub> (1.5 mM), CaCl<sub>2</sub> (2 mM), D-glucose (10 mM) and HEPES (20 mM); pH adjusted to 7.4 and filtered with 0.45 μm Nylon filters prior to use. Pt wires (diameter 0.5 mm, high purity 99.99+ %) were bought from Goodfellow (OAKDALE, PA).

### **2.2.2 Cell culture and preparation**

A549 Human Lung Carcinoma cells (adherent, epithelial and with a doubling time ~22 hours) were cultured in BME supplied with 10% FBS, 2 mM L-glutamine, 100 units/ml penicillin and 100 μg/ml streptomycin. Cells were grown in 75-cm<sup>2</sup> cell culture flasks (Nunc\* Sterile EasYFlask) in a CO<sub>2</sub> cell culture incubator (HERA cell incubator, Newtown, CT) at 37 °C and

5% CO<sub>2</sub>, and were subcultured when reaching ~ 80% confluency every 3-4 days. Cells were counted with a Hauser Bright-Line Phase counting chamber to get a seeding density of  $1 \times 10^7$  cells / 75 cm<sup>2</sup> in culture flasks. Before the experiments, cells were plated on 35-mm gridded uncoated glass-bottom cell culture dishes (MatTek Corp., Ashland, MA) in a seeding density of  $1.8 \times 10^4$  / 962 mm<sup>2</sup>. Experiments were performed on the second and third days following the cell plating.

## **2.2.3 Cell fluorescence staining**

### **2.2.3.1 Staining for SCEP observation**

The cells were stained with cell-permeable calcein AM or Thioglo<sup>®</sup> 1 for flow-out-of-cell visualization. Cell-impermeable propidium iodide (PI) was used for taken-up visualization.

Thioglo<sup>®</sup> 1 is a non-fluorescent maleimide-based reagent that gives a highly green fluorescent product upon its reaction with active SH groups in proteins, enzymes, and small peptides [116]. When cells were treated with Thioglo<sup>®</sup> 1, the triggered-on fluorescence was ascribed to GSH- Thioglo<sup>®</sup> 1 adduct [117], thus Thioglo<sup>®</sup> 1 can be used for detection and titration of GSH, which plays a vital anti-oxidation and free-radicals-remover role in cell functions and metabolism. The Thioglo<sup>®</sup> 1-GSH adduct has an absorbance  $\lambda_{\text{max}}$  at 379nm and emission  $\lambda_{\text{max}}$  at 513 nm. Low concentration of Thioglo<sup>®</sup> 1 (< 10  $\mu\text{M}$ ) was reported to be non-cytotoxic [117]. For staining, cells were washed 3 times by extracellular buffer and stained with

2  $\mu\text{M}$  Thioglo<sup>®</sup> 1 in 0.5 ml extracellular buffer for 30 s at room temperature, then washed again and finally bathed in the extracellular buffer for electroporation.

Calcein AM is a widely used green-fluorescent cell marker for the studies of cell membrane integrity and for long term cell tracing. It is a non-fluorescent, cell permeant compound that can be hydrolyzed by intracellular esterases into the green-fluorescent anion calcein (absorbance  $\lambda_{\text{max}}$  at 494nm, emission  $\lambda_{\text{max}}$  at 517 nm) in living cells. Cells were stained with 1  $\mu\text{M}$  calcein AM in 2 ml culture media for 1 hour at 37 °C and washed with extracellular buffer before employed in electroporation.

PI is a popular red-fluorescent nuclear and chromosome counterstain (absorbance  $\lambda_{\text{max}}$  at 536nm, emission  $\lambda_{\text{max}}$  at 617 nm). This membrane impermeant dye stains by intercalating into nucleic acid molecules between the bases with little or no sequence preference. It binds both DNA and RNA. PI is also commonly used for identifying dead cells. When using PI as an indicator of electroporation, the electroporation media was replaced by 2  $\mu\text{M}$  PI in 2 ml extracellular HEPES buffer.

### **2.2.3.2 Cell viability check**

After electroporation, the viability of cells was examined by fluorescent kits calcein AM and /or PI. Cells pre-stained with Thioglo<sup>®</sup> 1 were exposed to both 0.5  $\mu\text{M}$  calcein AM and 0.5  $\mu\text{M}$  PI in 2 ml culture media at 37 °C for 40 min. If cells were pre-stained by calcein AM, only PI was used to identify dead cells. When electroporation was conducted in the presence of PI, calcein AM staining helped to tell integrity of the cell membrane after electroporation.

#### 2.2.4 EFC fabrication and buffer filling

We adopt pulled capillaries for electroporation. The benefits compared to the unpulled capillaries are: (1) higher spatial resolution; (2) lower voltage is required because the voltage drop concentrates at the cell tip region; (3) decrease the osmotic flow; (4) potentially smaller volume for delivery.

The fabrication of EFC with pulled tips was done in a clean hood. Fused-silica capillaries from Polymicro Technology (Phoenix, AZ) were used. The dimensions of the fused-silica capillary were o.d. 367  $\mu\text{m}$  and i.d. 100  $\mu\text{m}$ . Capillaries were pulled at one end by using a  $\text{CO}_2$  laser puller (Sutter Instruments Co. P-2000, Novato, CA). Before the capillary was pulled, a 2-cm-center section of a 35-cm-long capillary was burned with flame to remove the protective polyimide coating, then flushed with filtered Milli-Q water (filtered by an online pre-column 0.2  $\mu\text{m}$  filter) and carefully truncated at the ends to get a final length of 30 cm with a Shortix™ fused-silica tubing cutter. These capillaries were pulled using four-line programs as listed in Table 2.1 to create reproducible capillaries with a short pulled tip having an i.d. of 4-5  $\mu\text{m}$  or  $\sim 2$   $\mu\text{m}$  (Figure 2.3). The final length of the capillary was 15 cm.

Before the experiments, the capillaries were filled with extracellular HEPES buffer by a plastic syringe. An online pre-column filter was put between the syringe and the capillary to eliminate the possibility of capillary clogging induced by particulates in the solution. The high pressure caused by the small tip requires an airtight flow from the syringe to the capillary.

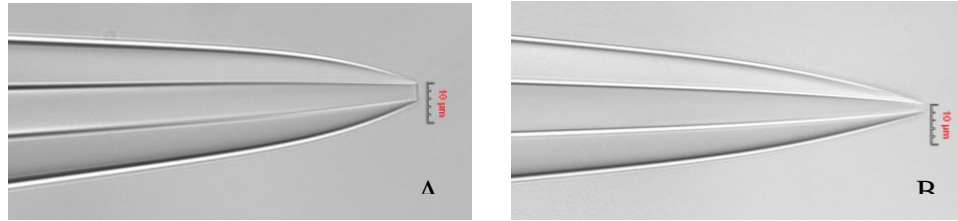


Figure 2. 3: Pictures of pulled capillaries under microscope (40 $\times$ ). The taper length is about 2 mm. (A) i.d. 4-5  $\mu\text{m}$ . (B) i.d.  $\sim 2 \mu\text{m}$ .

Table 2. 1: Programs for capillary pulling

Line No.	4-5 $\mu\text{m}$					$\sim 2 \mu\text{m}$				
	Heat	Filament	Velocity	Delay	Pull	Heat	Filament	Velocity	Delay	Pull
1	250	0	30	200	0	250	0	30	200	0
2	250	0	30	200	0	250	0	30	200	0
3	250	0	30	200	0	250	0	30	200	0
4	254	0	30	200	0	270	0	30	200	0

### 2.2.5 Microscope imaging

The cell dish was fixed in a cell chamber (DH 35i culture dish incubator, Warner Instruments, Holliston, MA) mounted on the stage of an inverted fluorescence microscope (Olympus IX 71, Melville, NY) coupled with a CCD (ORCA-285 IEEE 1394 -Based Digital Camera, Hamamatsu Photonics K.K., Japan) for fluorescence imaging. A HBO 100 W mercury lamp in the microscope was used as the excitation source. Cells were observed through a 20x 0.70 NA UPlanApo objective lens. Image processing was performed by the image acquisition software

SimplePCI from Compix Inc (Sewickley, PA). Fluorescent Intensity was corrected by background deduction.

For Thioglo<sup>®</sup> 1, an Omega fluorescence filter cube (especially built, exciter XF1075-387AF28, dichroic XF2004-410DRLP, emitter XF3087-480ALP, Omega Optical, Brattleboro, VT) was used for excitation at 378 nm and emission at 480 nm. For calcein AM and PI imaging, BrightLine<sup>®</sup> DA/FI/TX-3X-A triple band pinkel filter set from Semrock (Rochester, NY) was used (exciter 1, 387 nm; exciter 2, 494 nm; exciter 3, 575 nm; emission, 457, 530, 628 nm). In electroosmotic flow study, a filter cube for calcein was used.

## **2.3 INSTRUMENTATION FOR SCEP WITH EFC**

### **2.3.1 Circuit design and electronics**

The experimental setup is depicted in Figure 2.4. It comprises two switchable circuits: electroporation circuit and test circuit. When doing experiments, the test circuit helps to examine the status of capillaries (clogging problem, resistance) and set the tip-cell distance via current measurement. After desired distance and satisfactory capillary status are obtained, the switches are altered to activate the electroporation circuit for electroporation accompanied with current monitoring.

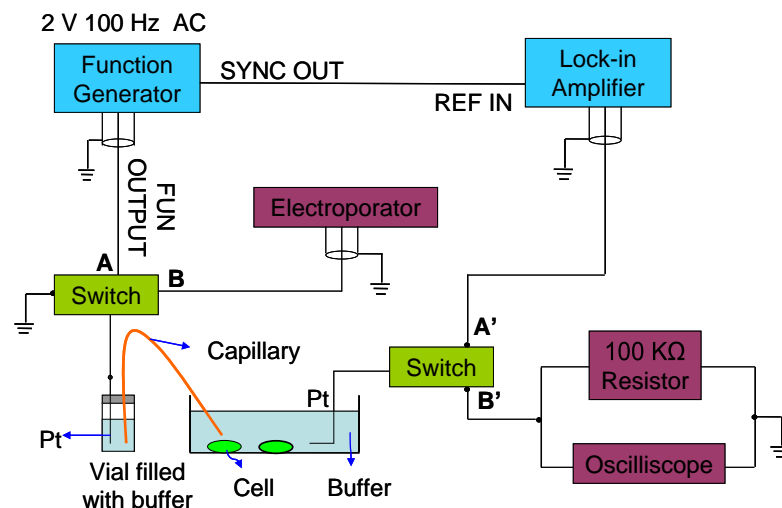


Figure 2. 4: Schematic diagram of the experimental setup. Two circuits, electroporation with current monitoring and test circuit are switchable from each other. By switching from A to B and A' to B', the active circuit converts from the test circuit to the electroporation circuit.

### 2.3.1.1 Electroporation circuit

When the switches were put in B and B' position, the electroporation circuit was in active. The 15-cm-long pulled capillary was positioned using a MP-285 motorized micromanipulator from Sutter (Novato, CA). The tip end was carefully placed near the target cell at a desired distance. The other end of the capillary was inserted into a vial filled with extracellular HEPES buffer. A platinum electrode placed in this vial was connected to the electroporator (BTX<sup>®</sup> ECM 830, Harvard Apparatus, San Diego, CA), and the electrical circuit was completed with another platinum electrode placed in the cell dish connecting to an added 100 kΩ resistor and oscilloscope (NI 5911 Digital Oscilloscope for PCI, National Instruments Corp. Austin, Texas) for current monitoring.

The added resistor was chosen to be 100 k $\Omega$  in order to (1) meet the measurement limitation of the oscilloscope (Max. 10 V), (2) minimize noise/signal ratio, (3) minimize the effect of the supplementary part to the whole electroporation circuit, that is, to minimize the resistance from the supplementary part. Since the resistance of EFC was always > 10 M $\Omega$ , the extra 100 k $\Omega$  resistor barely affected the electroporation current. Ignoring the other impedance sources, the expected reading in oscilloscope is given by (the oscilloscope has an input impedance of 1 M $\Omega$ ),

$$V_{oscilloscope} \approx \frac{V_{apply}}{R_{EFC} + R_{supplementary}} \times R_{supplementary} = V_{apply} \times \frac{0.091M\Omega}{R_{EFC} + 0.091M\Omega}$$

In our experiments, the applied voltage for electroporation was a single DC square wave having a magnitude of 500 V and duration of 300-400 ms; the current flowed through with a rising time of ~ 200  $\mu$ s and a decay time of ~ 300  $\mu$ s.

The distance between the tip and cell  $d$  for electroporation was 3.5 or 4  $\mu$ m and determined in two ways. One was by putting a scale bar to visually measure the distance, and this observed distance between the capillary tip and the cell was the projection of the images in the horizontal imaging plane (cell dish surface). The other way was to find the cell-tip touching point *via* current measurement followed by horizontal retreat to obtain the desired distance.

### 2.3.1.2 Test circuit

The test circuit helped to learn the behavior of the capillary. The other function of it was to help control the distance between cell and tip by defining the touching point. Besides the Pt wire-vial filled with buffer-EFC-cell dish-Pt part, this circuit also included a synthesized function

generator (SRS Model DS 340, Stanford Research Systems, Inc., Sunnyvale, CA) and a lock-in amplifier (SRS Model SR 830 DSP). The function generator gave a continuous 2 V AC signal at 100 Hz. This signal passed through EFC and cell dish and was finally captured by lock-in amplifier. The lock-in amplifier was set to lock the specific frequency by input of the signal from function generator to the reference channel, thus measured the current of the whole circuit at this specific frequency. Those unwanted noise at other frequencies were eliminated.

When the capillary tip was away from the cells, the current reading from lock-in amplifier provided information of capillary resistance, helped to examine if the capillary was clogged or the capillary size was satisfied. In the case when tip was approaching to the cell, the current told us how close the distance was; in this way, we can determine the tip-cell touching point and control the distance by retreating the tip from the cell with a micromanipulator.

### 2.3.2 EFC resistance

Resistance of the EFC can be estimated by the current reading from lock-in amplifier when capillary tip was away from cells:

$$R_{EFC} \approx \frac{2 V}{I \text{ (reading from Lock - in Amplifier)}}$$

Because this calculated resistance also contained resistance from the buffer solution in vial/cell dish and electronics, it was always larger than the real value. The above estimation was based on the fact that the total resistance of the vial/cell buffer and electronics were much smaller than the EFC resistance (several k $\Omega$  compared to > 12 M $\Omega$ ).

We tested the pulled capillaries' resistance with different tip sizes. Under the situation that EFC with a 2- $\mu\text{m}$  tip was clear and desirably sized, the experimental reading from lock-in amplifier was 0.12 ~ 0.13  $\mu\text{A}$ , which corresponded to a resistance of ~ 16  $\text{M}\Omega$ . When the tip grew to 4-5  $\mu\text{m}$ , the reading increased to 0.13 ~ 0.14  $\mu\text{A}$  corresponding to ~ 14  $\text{M}\Omega$ . These were very close to the simulated values (see simulation part). If the capillary was clogged, the reading decreased a lot. Therefore we were able to select a suitable sized capillary without clogging before carrying out electroporation by simply reading from the lock-in amplifier.

### **2.3.3 Current measurement controlled tip-cell distance**

As mentioned in 2.2.2, we can control the tip-cell distance by current measurement in test circuit. When the capillary tip was touching the cell, a seal was formed. Cell membranes have been reported to have affinity to substrate materials such as glass [96]. In patch-clamp technology, people have been using glass pipets having an opening of 0.5 ~ 1  $\mu\text{m}$  to create a giga-seal on cells to study the electrophysiological behavior of ion channels [118, 119]. In our case, the tip was larger, and a smaller seal was expected. Figure 2.5 shows how the system resistance in test circuit changes when the tip approaches to the cell.

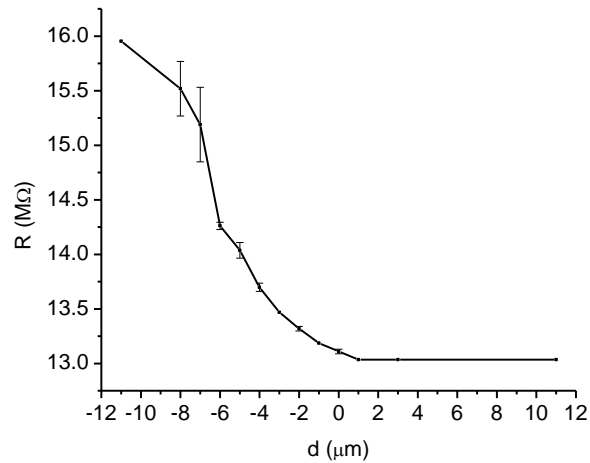


Figure 2. 5: Resistance changes when a 5  $\mu\text{m}$  capillary tip seals with cell membrane. We set the point when the resistance begins to change as distance zero. Based on the microscope observation and simulation, this zero point is extremely close to the touching point.

Relying on the reading from lock-in amplifier, we were able to tell a change of  $> 2\%$ . In the following simulation part, we found that this extent of change happened only when the distance decreased to zero. A deeper indent enhanced the resistance change, which helped to tell the real change from the already weakened noise. Combined with a high resolution micromanipulator, we were able to find the zero distance point, and then retreated from the point to get a desired distance.

A significant advantage of this distance control method over the scale bar measurement is that higher spatial resolution can be achieved. Usually the scale bar method is limited beyond 1  $\mu\text{m}$ . With the current measurement method, the limitation mainly comes from the noise and micromanipulator. A high resolution micromanipulator can possibly help to obtain a spatial

resolution of 0.1  $\mu\text{m}$ . Some other advantages are (1) the freedom to approach the EFC from any angle to the cell; (2) the distance is not necessary the projection one on the horizontal plane (this may induce distance variance by the gap between the tip and cell dish), it can be a direct distance between the tip and cell.

## **2.4 NUMERICAL SIMULATION**

As mentioned before, the inhomogeneous electric field makes analytical calculation difficult. The Orwar group gave analytical formula for electric field distribution at the symmetric axis produced by a uniform i.d. capillary. However, we are using a pulled capillary; hence the situation of electric field distribution is much more complicated. Predecessor in our lab has developed a numerical simulation model for SCEP in Comsol Multiphysics 3.3, and used the model to anticipate the FEA and TMP. Here we applied the similar method for numerical study of SCEP, capillary resistance and electric field distribution.

### **2.4.1 Model setup and parameters**

#### **2.4.1.1 Capillary drawing in Comsol**

A typical capillary with a 2  $\mu\text{m}$  tip opening and a taper length of 2 mm was chosen for real capillary drawing in the model. Because the length of capillary (15 cm) was much larger than the tip opening, only part of the capillary, including the tapered 2 mm and 0.5 mm unpulled

section ( $L=2$  mm,  $l=0.5$  mm in Figure 2-6) was modeled. The real dimensions (o.d./i.d. ~ distance from the tip end) were measured after taking images under 20x, 40x, and 60x. These data were imported into OriginLab and fitted into 3 Sigmoidal Boltzman functions (0-100  $\mu\text{m}$ /100-600  $\mu\text{m}$ /600-1600  $\mu\text{m}$ ) for smoothing. The joint parts were either fitted with blended functions or corrected based on the real data. Finally 62 points were given to structure the capillary for inner wall and outer wall, separately. For comparison, a model with a capillary of 3.6  $\mu\text{m}$  was also built in the similar way.

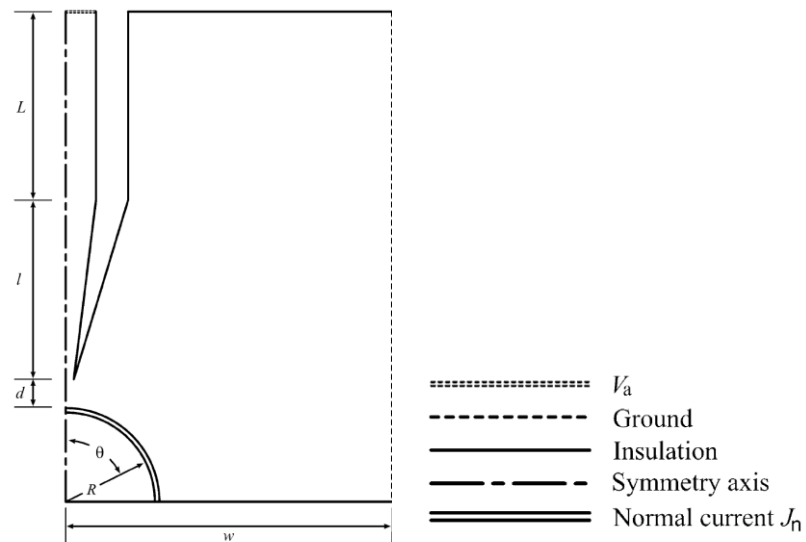


Figure 2. 6: SCEP modeling geometry. Boundary conditions, defined by line styles, are described in the figure. The capillary is positioned perpendicular to the dish surface and is centered above the cell. Rotational symmetry is used to simplify the simulation. In simulations, the actual shape of the capillary tip shown in Figure 2.1 (B) is used. Components are not drawn to scale [113]. © 2007 by the Biophysical Society

### 2.4.1.2 Model and parameters

Table 2. 2: Parameters and constants

Total capillary length $L_{tot}$	0.15 (m) or 0.10 (m)
Simulated capillary length $L_{sim}$	0.0025 (m)
Applied voltage $V_{app}$	500 (V)
Conductivity of extracellular buffer $\sigma_s^*$	$C_A + C_B(T - 273.15) + C_C(T - 273.15)^2$ (S/m)
Conductivity of cytoplasm $\sigma_c$	$\frac{13}{60} \times \sigma_s$ (S/m)
Conductivity of cell membrane $\sigma_m$	$5.3 \times 10^{-5}$ (S/m)
Cell membrane thickness $\Delta$	$7 \times 10^{-9}$ (m)
Critical TMP	0.25 (V)
Tip-Cell distance $d$	0.5 ~ 8 ( $\mu\text{m}$ )
Cell radius $R$	Small cells $R = 10 \mu\text{m}$ , Median cells $R = 12.5 \mu\text{m}$ Large cells $R = 20 \mu\text{m}$

\* *The value of  $\sigma_s$  was measured by applying an electric potential across two electrodes (plates) immersed in a test solution under different temperature and fitted into a polynomial curve.  $C_A=1.11669$ ,  $C_B=0.01838$  and  $C_C=1.65 \times 10^{-4}$ .*

The simulation of SCEP utilized a conductive Media DC with 2D axis-symmetric. This model solved a partial differential equations (PDE):  $-\nabla(\sigma \nabla V) = Q$ , where  $\sigma$  is the

conductivity and  $Q$  is the current source. Figure 2.6 shows the modeling geometry and boundary conditions. Parameters and constants used are listed in Table 2.2. Two model navigators,  $d_{cout}$  and  $d_{cins}$ , separate the inside cell and outside cell domains. They are related by membrane boundary condition set to be  $J_n(d_{cout}) = (V_i - V_o) * \sigma_m / \Delta$  and  $J_n(d_{cins}) = (V_o - V_i) * \sigma_m / \Delta$ . The voltage at the simulated capillary unpulled end is related to the applied voltage with the equation,  $V_0 = V_{app} + E_{y\_dcout} \times (L_{tot} - L_{sim})$ . Accurate calculation of  $V_0$  requires to turn on the ‘‘weak boundary condition’’.

A simplified model comprising only a capillary in the whole geometry simulated the resistance of capillary. A potential was applied at the top end and the capillary tip end was set as ground.

#### **2.4.2 Potential and electric field distribution near the EFC tip**

Figure 2.7 shows how the potential and electric field distribute near the tip when a capillary having a 2  $\mu\text{m}$  tip is put 15.5  $\mu\text{m}$  away from the cell dish surface. With an apply voltage of 500V, approximately 75% potential drop happens in the untapered section, and more than 20% voltage drop occurs exponentially at the 2 mm tapered section. At the tip where in the figures corresponding to  $d = 0$ , the potential is only several volts. The existence of cell barely affects the potential drop across the capillary (plot (C) and (D)). Placing a cell under the capillary induces the formation of a sharp potential drop across the cell membrane (plot (D) insets).

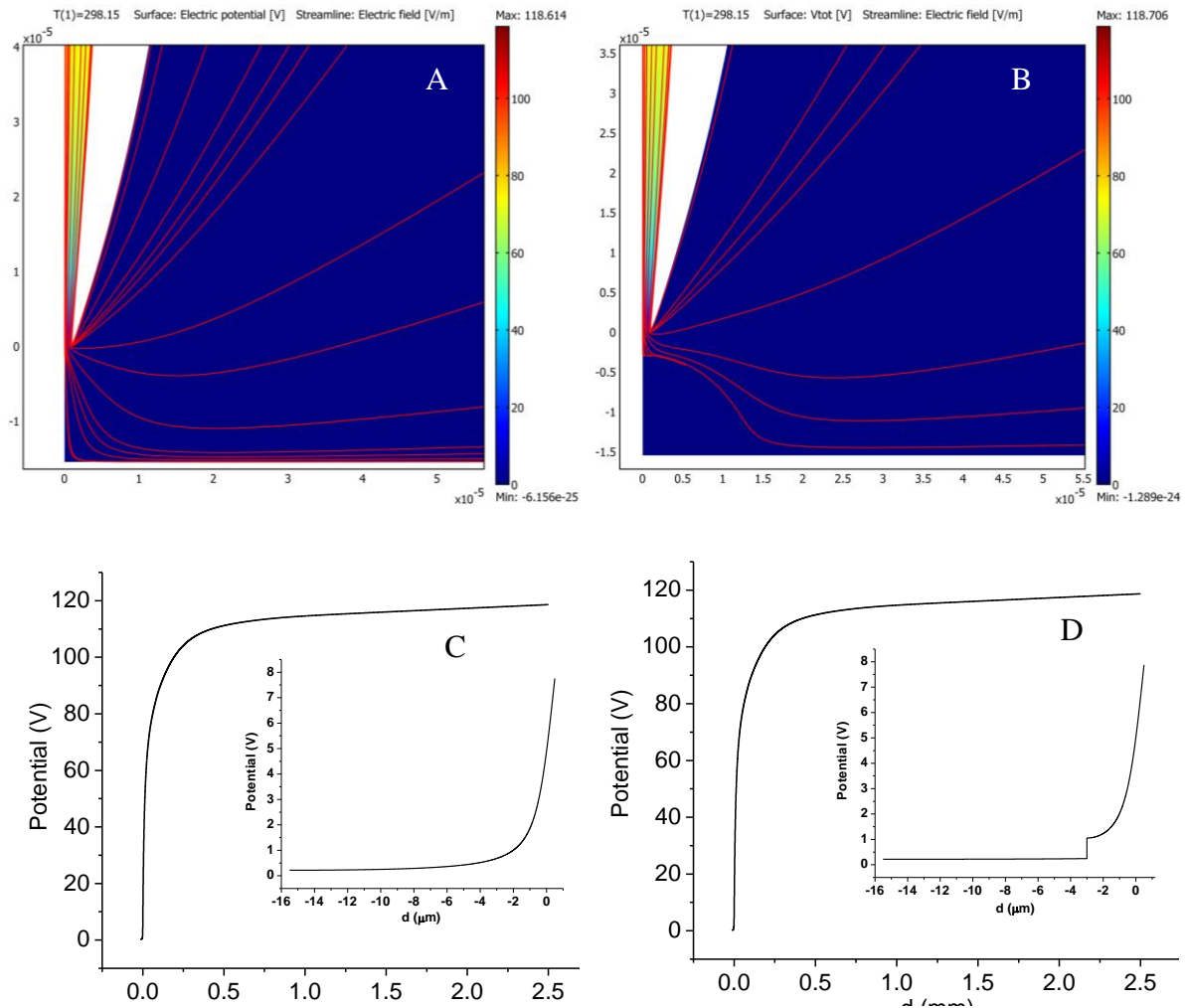


Figure 2. 7: Simulated electric field and potential distribution. (A) and (C): no cell; (B) and (D): with a median-sized cell. (A) and (B) show the surface plots for potential distribution and streamline plots for electric field distribution around the 2 μm tip. (C) and (D) are the potential drop curves along the central axial of capillary, with insets for the extension into the solution/cell.

The streamline plots in Figure 2.7 indicate an intense electric field at the tip and an exponentially dropping electric field when going farther into the bath buffer (plot A). The electric field is distorted by the presence of a cell (plot B).

### 2.4.3 Resistance for EFC with different tip size

The capillaries with tip i.d. of 2  $\mu\text{m}$  and 3.6  $\mu\text{m}$  were simulated by simply setting the top end with a potential source of 500V and the tip end as grounding. The resistance of EFC was then calculated by

$$R = \frac{U}{A} = \frac{U}{\int J} = \frac{500(V)}{\int J_z - dc(A)}$$

where J is the current density across the lumen of the capillary.

Table 2.3 gives the resistance of these two different tip-sized capillaries at different temperature. Apparently the resistance decreases along with the increase of temperature because of the enlarged conductivity. The resistance of 2  $\mu\text{m}$  tip capillary is slightly larger than 3.6  $\mu\text{m}$  one. At room temperature, they give resistance of 14.5 M $\Omega$  and 13.7 M $\Omega$  respectively.

Table 2. 3: Simulated resistance of different tip-sized capillaries at different temperature

T ( °C)	2 μm tip capillary		3.6 μm tip capillary		Difference	
	Resistance	Reading *	Resistance	Reading	Resistance	Reading
	(MΩ)	(μA)	(MΩ)	(μA)	(MΩ)	(μA)
0	21.87303	0.09144	20.61623	0.09701	1.2568	0.00557
15	17.08537	0.11706	16.10472	0.12419	0.98065	0.00713
20	15.75421	0.12695	14.85008	0.13468	0.90413	0.00773
25	14.5434	0.13752	13.70913	0.14589	0.83427	0.00837
30	13.44442	0.14876	12.67316	0.15781	0.77126	0.00905
37	12.07474	0.16563	11.38215	0.17571	0.69259	0.01008

\* *Reading: Calculated reading from lock-in amplifier given the function generator produces 2 V<sub>rms</sub> without considering the other sources of resistance.*

#### 2.4.4 Resistance with cells at various tip-cell distances

Using the same model for SCEP simulation, the resistances of EFC and the whole electroporation system were calculated by the voltage drop and integrated current

$$R(EFC) = \frac{\Delta U}{\int J(\text{Inlet end})} = \frac{500 - U(\text{tip center}) (V)}{\int J_z - dc(\text{Inlet end}) (A)}$$

$$\text{System resistance} = \frac{500 (V)}{\int J_z - dc(\text{Inlet end}) (A)}$$

By this method, we investigated the resistances of the two types of capillaries with presence of cells at various tip-cell distances at 25 °C. Table 2.4 shows results for the small cell with 2 μm tip capillary. The capillary resistances obtained in this model are similar to those in Table 2.3. The tip-cell distance changing from 100 μm to 0.5 μm induces no noticeable change of the resistance and current. A deeper inspection indicates that the change of resistance cannot be detected unless tip-cell distance is extremely small, as shown in Table 2.5 in terms of large cells, 2 μm tip capillary and short distance.

Table 2. 4: Resistance measurement in electroporation simulation model with small cells (R = 10 μm) and 2 μm tip EFC

Tip-cell distance (μm)	Voltage at tip (V)	Current Integration (μA)	Capillary Resistance (MΩ)	System Resistance (MΩ)	Current (μA)
100	4.84035	34.1064	14.51807	14.65999	0.13643
8	4.88908	34.1031	14.51804	14.66141	0.13641
1	5.66939	34.0539	14.51612	14.68261	0.13622
0.5	6.85438	33.9866	14.51001	14.71169	0.13595

Simulation with 3.6  $\mu\text{m}$  tip capillaries shows similar results. Though the real system resistance is larger than the simulated due to other resistance sources, this theoretical result still strongly supports our current measurement-based distance control method.

Table 2. 5: Short distance resistance measurement in electroporation simulation model with large cells ( $R = 20 \mu\text{m}$ ) and 2  $\mu\text{m}$  tip EFC

Tip-cell distance ( $\mu\text{m}$ )	Voltage at tip (V)	Current Integration ( $\mu\text{A}$ )	System Resistance ( $\text{M}\Omega$ )	Change (%)	Lock-in amplifier Reading ( $\mu\text{A}$ )
1	5.8022	34.0451	14.68641	0	0.136
0.5	7.10299	33.9704	14.71868	-0.16861	0.136
0.25	9.19321	33.8556	14.76859	-0.38853	0.136
0.125	11.65082	33.7166	14.8295	-0.72575	0.135
0	19.809961	33.1995	15.060048	-2.64643	0.133
Seal (-0.047)	29.134133	32.5574	15.35750	-4.53046	0.130
Dent -1	156.74168	24.0030	20.83069	-29.6166	0.096

#### 2.4.5 FEA and TMP for electroporation

This model also gives FEA and TMP as introduced in chapter 1. TMP corresponds to the difference value between the potential at the outside and inner side of the membrane, and FEA

is calculated by dividing the area where  $TMP \geq 0.25$  V by the whole cell area. Shorter distance means higher TMP and larger FEA. The simulated electroporation behavior at different tip-cell distances with 2  $\mu\text{m}$  and 3.6  $\mu\text{m}$  tips was demonstrated in Figure 2.2.

## 2.5 ELECTROSMOTIC FLOW DURING ELECTROPORATION

The EFC we used is a fused-silica capillary without any modification in the inner wall; therefore because of the negative-charged characteristic of silica surface, electroosmotic flow is a factor that may affect the electroporation. An experimental observation of this effect was that a neutral molecule can move out of the capillary tip into the buffer bath when the external applied current flowed from the unpulled inlet towards the pulled tip.

Electroosmotic flow phenomena were studied using Invitrogen FluorSphere® beads labeled by NeutrAvidin™ (Polystyrene microsphere, diameter 0.04  $\mu\text{m}$ , yellow-green fluorescent ex505/em 515). The isoelectric point (PI) of NeutrAvidin™ is 6.3. The beads are close to neutral in pH 7.4 extracellular buffer. Before experiments, the beads solution were sonicated, mixed with HEPES extracellular buffer at random concentration, filtered by 0.11  $\mu\text{m}$  Nylon filter and filled into the EFC with the aid of a syringe. The EFC was then used for electroporation setup. Electroosmotic flow was observed while applying a single pulse or a train of pulses at different durations and frequencies. Figure 2.8 is a fluorescence picture of a beads-filled EFC tip immersed in the buffer solution. The mean fluorescence intensity change within the red circle for different sized tips (2, 4 and 6  $\mu\text{m}$ ) was measured (Figure 2.9).

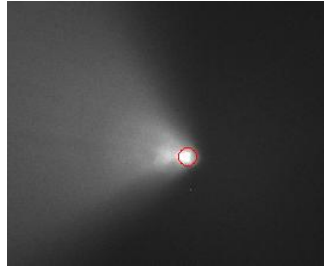


Figure 2. 8: A picture of fluorescent-beads-filled capillary for electroosmotic flow study

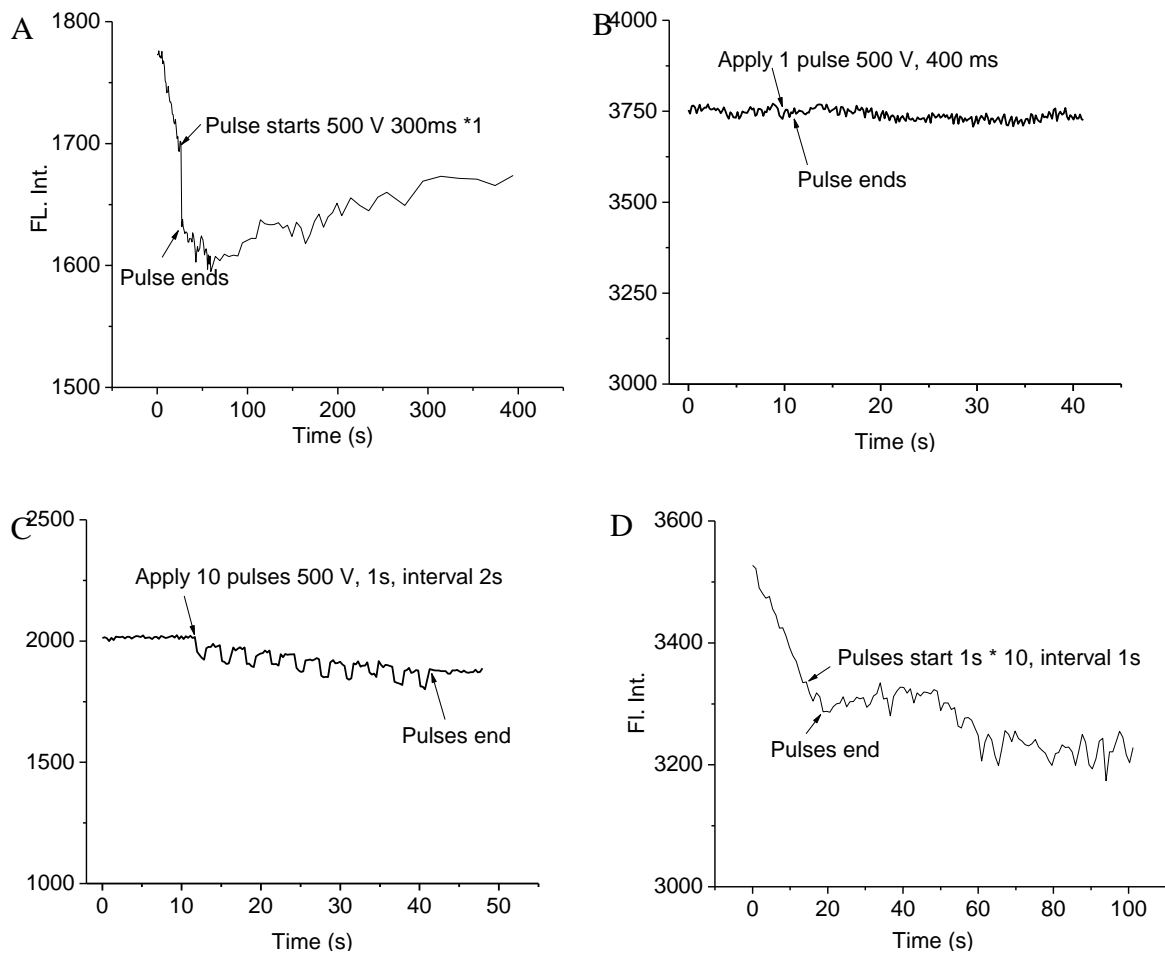


Figure 2. 9: Fluorescence intensity change within the focused tip portion when pulses are applied on the fluorescent-beads-filled capillaries. (A) 2  $\mu$ m tip, a single 300 ms pulse of 500

V; (B) 4  $\mu\text{m}$  tip, a single 400 ms pulse of 500 V; (C) 4  $\mu\text{m}$  tip, a train of 1 s pulses of 500 V; (D) 6  $\mu\text{m}$  tip, a train of 1 s pulses of 500 V.

A sharp decrease in Figure 2.9 (A) indicates a noticeable electroosmotic flow when a 2  $\mu\text{m}$  capillary tip is exposed under the experimental electroporation pulse conditions (a single pulse, 300-400 ms, 500V). With the similar pulses, a 4  $\mu\text{m}$  tip shows no obvious intensity change (Figure 2.9 (B)). However, stronger pulses enhance the electroosmotic flow (Figure 2.9 (C)). When the tip size continues to increase, the electroosmotic flow keeps fading away (Figure 2.9 (D)).

Based on above results, we conclude that smaller tips have larger osmotic flow than large tips in the range of 2-6  $\mu\text{m}$ . When tip opening is larger than 4  $\mu\text{m}$ , no noticeable electroosmotic flow occurs at a single short pulse (300-400ms) which is usually applied for electroporation. An explanation for this is that smaller tip has much larger electric field at the tip. In the future, we will investigate deeper into the electroosmotic flow and electrophoresis during electroporation with the aid of Comsol numerical simulation. If necessary, we can coat the capillary with polysaccharides to suppress the electroosmotic flow. An advantage from the electroosmotic flow is that it can help to deliver the loading agent into cells.

## 2.6 ELECTROPORATION RESULT

### 2.6.1 Excellent spatial resolution

An excellent spatial resolution was obtained with such a small EFC tip. Neighboring cells are never electroporated throughout the whole electroporation experiments, even when there is no gap between the target cell and its neighbors. Figure 2.10 shows a fast temporal resolution electroporation of a target calcein AM-stained cell 1.1 without affecting the adjacent cell 1.2.

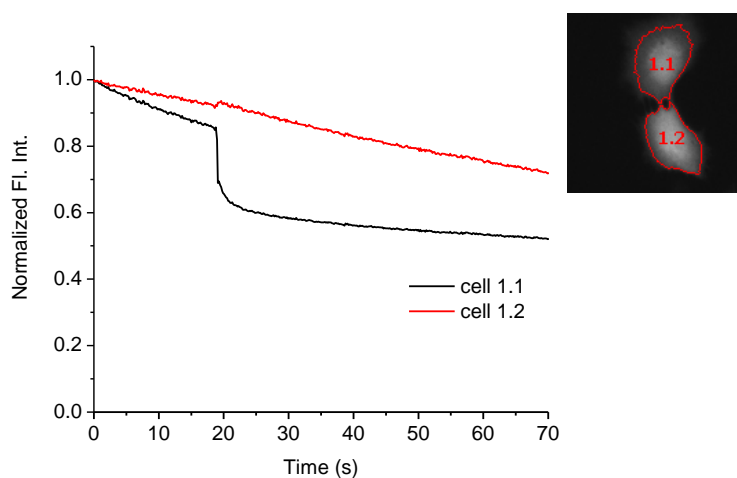


Figure 2. 10: High spatial resolution of electroporation with a 2  $\mu\text{m}$  tip EFC. The sharp jump of fluorescence intensity in cell 1.1 indicates electroporation, while cell 1.2 only shows photobleaching under exposure to light.

## 2.6.2 Fluorescence exposure and dye selection affect cell viability

We reveal that the fluorescence exposure dose affects the survivability of electroporated cells. Two kinds of imaging manners were adopted. One was taking fluorescence sequences in a speed of 1 frame / second, the other was only snapping fluorescence images right before applying the pulse and 2 min after electroporation. In both manners, the microscope was set to minimize photobleaching. Table 2.6 gives the success electroporation rate and survival rate of the target cells when a tip-cell distance of 3.5  $\mu\text{m}$  is applied under these two imaging manners. Although similar success rates are obtained, the reduced light exposure from two single-snaps significantly improves the survivability of cells. This could be a result of the creation of hazard radicals upon photobleaching.

Table 2. 6: Summary of cell electroporation success and survival results at  $d = 3.5 \mu\text{m}$

Imaging manner	Number of Cells				Success rate	Survial rate
	Success	Fail	Alive	Dead		
Sequence imaging	57	17	18	56	77%	24%
Two single-snaps	39	10	24	25	80%	49%

The selection of dyes may also influence the survivability of cells. One fact is that electroporation under PI staining yields more living cells than Thioglo<sup>®</sup> 1 (80% survivability with 93% success rate with 14 cells). The reason is unclear. One guess could be that in Thioglo<sup>®</sup> 1 experiments, cells were pre-stained before exposure to lights, while PI entered the

cells after electroporation. The other explanation could be that the photobleaching of Thioglo<sup>®</sup> 1-induced fluorescence is very fast, thus more hazard radicals are produced. Furthermore, the cytotoxicity of dyes affects cell viability. Calcein AM staining is reported to be toxic to some cancer cells [120-122]. Our cell cytotoxicity studies also show that the calcein AM-stained cells were induced to death after fluorescence exposure when soaked in extracellular HEPES buffer for 2.5 hours. Thus despite the brighter fluorescence and lower photobleaching, calcein AM is not suitable for cell survivability examination after electroporation. We only used calcein AM staining to obtain high temporal resolution imaging, trying to get some dynamic information during electroporation.

### 2.6.3 SCEP with Propidium Iodide staining

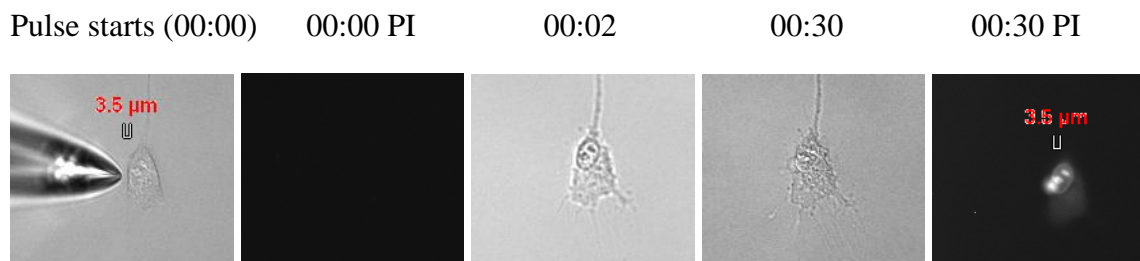


Figure 2. 11: PI uptake in SCEP

The cell membrane-impermeable PI was used in our experiments to validate the pore formation by uptake of PI into induced cells when applying the pulses. The electroporation was conducted with EFCs having 2 μm tips. A single 300 ms pulse of 500 V was applied while keeping the tip-cell distance 3.5 μm. Figure 2.11 shows that PI penetrates into a cell upon

electroporation and stains mainly the nuclear part. Most cells maintain viability after electroporation. From the bright field images, subcellular arrangement happens when the pulse is applied followed by a slow recovery phase.

#### **2.6.4 Fast temporal resolution imaging**

Calcein AM staining produces a bright fluorescence with less photobleaching than Thioglo<sup>®</sup> 1 staining. Therefore we used calcein AM for high temporal imaging, trying to capture some dynamic information of electroporation. The EFC was placed at the top of cells right above the smaller circle in Figure 2.12. An average imaging rate of 5 frames / second was achieved. The normalized fluorescence intensity changes of the whole cell and the tip part were plotted as a function of time (Figure 2.12). Both 2  $\mu\text{m}$  and 4  $\mu\text{m}$  tips shows similar curve shapes. The whole cell has a smooth dropping curve while the tip part has some sudden drop in a time scale of several hundred milliseconds followed by a small recovery.

One explanation of this interesting tip phenomenon could be that the electroosmotic flow brings fluorescent substances into the cells. It could also contain dynamic information of electroporation: pores opening at the tip part induce a sudden flow-out of fluorescent substances in expansion phase; then diffusion inside the cells complements this sudden loss during the stabilization and resealing phases. Coating capillary inner wall to eliminate the electroosmotic flow is required for further investigation.

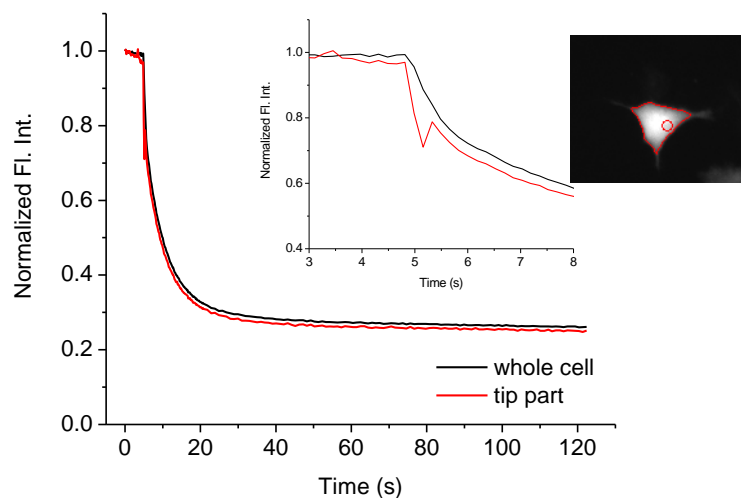


Figure 2. 12: Normalized fluorescence intensity changes in calcein AM-staining fast temporal resolution SECP. The inset magnifies the short pulse applying period. Red curve corresponds to the small circle right below the tip in electroporation, black one is for the whole cell.

## 2.6.5 Technical issue limits distance control and small tips

### 2.6.5.1 Preliminary electroporation results

Electroporation using different tip sizes and different distance control methods were preliminarily tested. Cells were stained with ThioGlo<sup>®</sup> 1 before electroporation. For comparison, EFCs were placed on one side of cells at a dihedral angle of 45 degree to the cell dish surface. Since a distance  $> 4 \mu\text{m}$  did not yield a good electroporation success rate (data not

shown), a distance of 3.5  $\mu\text{m}$  was applied. Fluorescent images were captured in sequence at a rate of 1 frame / second.

As shown in Figure 2.13, the results are not satisfactory. Large variance still exists. Distance control by current measurement does not help to narrow the deviations. Moreover, contrary to our expectation, the 2  $\mu\text{m}$  tip opening does not help to improve the cell survivability by decreasing the loss of intracellular substances.

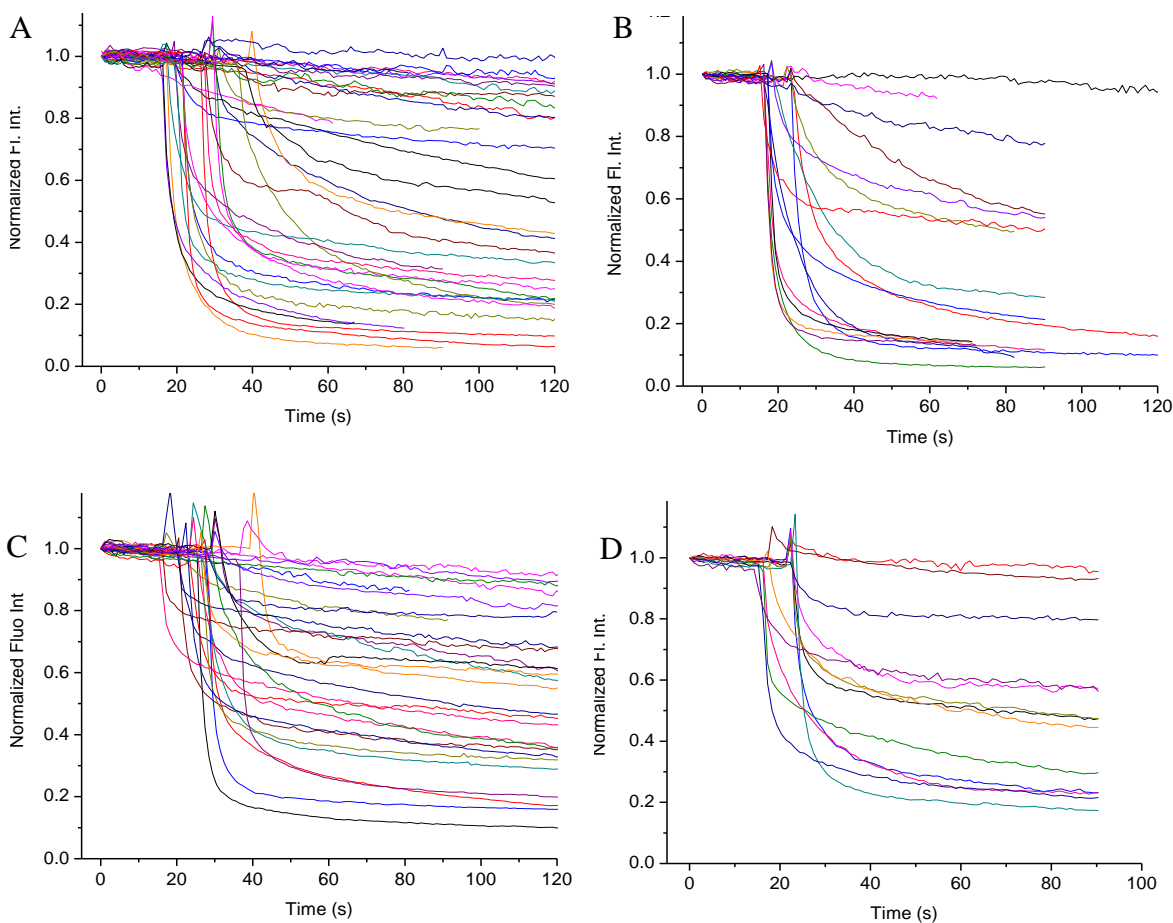


Figure 2. 13: Normalized fluorescence intensity changes in Thioglo<sup>®</sup> 1 - staining SECP.

Different tip sizes and tip-cell distance control methods are applied. (A) Tip opening 2  $\mu\text{m}$ ,

current control; (B) Tip opening 2  $\mu\text{m}$ , scale bar measurement; (C) Tip opening 3  $\mu\text{m}$ , current control; (D) Tip opening 3  $\mu\text{m}$ , scale bar measurement.

Table 2. 7: Success and viability in SCEP with different cell sizes and shapes

Cell No.	Diameter	Length	Breath	Roundness	Greylevel		F.I.	Success	Viability
	( $\mu\text{m}$ )	( $\mu\text{m}$ )	( $\mu\text{m}$ )		Start	End	Change		
1	19.73	44.67	6.84	0.36	12891	12946	<b>0.4%</b>	-	alive
2	23.17	39.13	10.78	0.53	26177	24679	<b>-5.7%</b>	-	alive
3	14.62	14.82	10.78	0.80	28674	26659	<b>-7.03%</b>	+	alive
4	21.29	53.536	6.65	0.31	20754	18827	<b>-9.3%</b>	+	alive
5	19.51	34.72	8.61	0.50	20731	17805	<b>-14.11%</b>	+	alive
6	21.43	30.97	11.65	0.62	19538	16686	<b>-14.6%</b>	+	alive
7	25.45	27.38	18.58	0.75	18946	15778	<b>-16.7%</b>	+	alive
8	24.66	24.65	18.66	0.80	26066	21100	<b>-19.1%</b>	+	alive
9	24.46	48.83	9.62	0.43	21279	10449	<b>-50.9%</b>	+	dead
10	23.23	68.37	6.20	0.23	22868	10404	<b>-54.5%</b>	+	dead
12	19.21	40.25	7.20	0.40	22967	6220	<b>-72.9%</b>	+	dead
13	13.72	15.86	9.33	0.73	33966	7966	<b>-76.5%</b>	+	dead

More experimental results without taking sequence imaging are shown in Table 2.7, which includes percentage loss of fluorescence and cell survivability for different cell sizes and shapes. It is clear that the cell viability depends on the fluorescence loss extent, which is highly related to the FEA. A loss above 50% induces the death of cells. However, the results show no

clue of the relationship between cell size and electroporation success rate and/or viability. More data are needed for statistical analysis.

So why don't the small tip and advanced cell-tip distance control benefit the electroporation yield? In principle, they should promote the yield. However in reality, two major technical difficulties are encountered in our current experiments: (1) the irreproducibility of size and shape of the capillary tips; (2) the backlash problem of the micromanipulator.

#### **2.6.5.2 Capillary reproducibility**

When preparing capillaries, reproducibility is an important issue. Although a part of unqualified capillaries can be found by the test circuit, a large variety of tip size and shape still exist with similar current readings. This technical issue matters more in the scope of 2  $\mu\text{m}$  tip capillaries than large tip capillaries considering the electric field distribution near the tips. In the future, we will use a high magnification objective lens for pre-experimental screening.

#### **2.6.5.3 Micromanipulator backlash**

Our present micromanipulator is gear-driven, and a backlash is produced when reversing the travel direction. This backlash is not reproducible and in a range of 0.2 ~ 2  $\mu\text{m}$ . The effect of backlash is disastrous as the distance control depends fully on the current measurement. Therefore, a piezo-manipulator is now under construction to obtain an accurate distance.

## 2.7 CONCLUSIONS

We have developed an integrated circuit not only for SCEP but also for pre-electroporation capillary testing and accurate distance control by current measurement. EFC with 2  $\mu\text{m}$  tips were constructed for SCEP with an intention for better control of small cells. High spatial resolution of electroporation was obtained. Fluorescence exposure time and dye types were found to affect the viability of cells. Uptake of PI into cells and sudden loss of intracellular fluorescence were indicative of success electroporation. High temporal resolution experiments revealed an abrupt fluorescence loss at a time scale of several milliseconds followed by recovery in the small portion of cell membrane facing the tip. Cell survivability was demonstrated to be related with the fluorescence loss. Comsol numerical 2D axis-symmetric simulation helped to reveal electroporation situation and support the distance control by current measurement. The preliminary testing of small tips and current measurement distance control did not provide satisfactory results, which may be a result of our current technical limitations.

## **3.0 FUTURE WORK**

### **3.1 CONTINUE WORK ON SURVIVABILITY AND VARIANCES PROBLEM**

#### **3.1.1 Piezo actuator for distance control**

A piezo actuator from Physik Instrumente will be attached to the present micromanipulator. The piezo has no backlash and has a travel distance of 30  $\mu\text{m}$ . In this way, we will solve the backlash issue and provide precise distance manipulation. A labview program will be set up for the piezo control, it will also enable the automation of finding the cell-tip touching point by telling the percentage of current drop in the test circuit.

#### **3.1.2 Temperature control by PDMI-2 micro-incubator**

Temperature effect on SCEP has never been studied. We will use a PDMI-2 micro-incubator from Warner Instruments to control the temperature of the cell dish and investigate how temperature affects electroporation. A suitable temperature based on the results will be chosen for maximization of electroporation efficiency and survivability.

### **3.1.3 Cell Synchronization**

To study the effect of synchronization and eliminate the variance caused by cell cycles, we will arrest A 549 cells with drugs. Several drugs have been applied for A 549 cell synchronization. A549 cells were synchronized in the very early S phase by a double thymidine treatment, in late G<sub>1</sub> using 600 μM of mimosine, at the G<sub>1</sub>/S boundary using 2 to 3 μg/ml of aphidicolin for 20 h or 4 mM hydroxyurea, and at M phase using 50 ng/ml of nocodazole for 30 h [123-125].

We are going to test above drugs for A549 cell synchronization. Cell synchrony will be monitored by DNA distribution assay, FACS analysis of the cells stained with propidium iodide after RNase digestion, which is a typical method for cell cycle assay. Cell survival with these drugs will be studied before applying the synchronized cells for electroporation. Once one or more effective drugs are selected, we will look into the influence of cell cycle on SCEP combining temperature control.

### **3.1.4 Working on other parameters**

Other parameters including pulse duration, tip-cell distance, cell size and shape will be studied and analyzed statistically. Also the imaging system will be improved to reduce the exposure time by coupling a cool CCD. Our final aim is to improve the cell electroporation efficiency and survivability, and decrease the variance between cells by parameters control.

### **3.2 DYNAMIC AND PORE INFORMATION STUDY**

Dynamic study and pore information study will be carried out for better understanding of SCEP. A sequence of imaging during electroporation gives resealing information. Fast resolution imaging helps to capture the transient alternation of the whole cell and subcellular organisms. Potential sensitive dyes can be used for real time detection of TMP.

The pore information including pores sizes and density will be studied by introducing fluorescent labeled macromolecules such as a series of different molecular weight fluorescence labeled dextrans into or out of the cells.

### **3.3 SECP OF OTHER CELL LINES**

Beyond A549 cells, other types of adherent cells will also be used for quantitative and qualitative study of SCEP. The facts revealed from one cell line will be tested on other line to finally achieve some general rules.

## BIBLIOGRAPHY

1. Puc, M., et al., *Techniques of signal generation required for electroporation. Survey of electroporation devices*. Bioelectrochemistry, 2004. **64**(2): p. 113-124.
2. Hooker, B.S., et al., *Production of human or human/porcine chimeric inactivation resistant coagulation factor VIII (FVIIIc) from plant cells and whole plants*. 2005: US. p. 23 pp , Cont -in-part of U S Ser No 588,314.
3. Swoboda, W., *Electroporation method and device for the disruption of plant cells to obtain juices*. 2007: EP. p. 23pp.
4. Terzaghi, W.B. and A.R. Cashmore, *Plant cell transfection by electroporation*. Methods in Molecular Biology 1997. **62**(Recombinant Gene Expression Protocols): p. 453-462.
5. Gallie, D.R., *Electroporation of RNA into Saccharomyces cerevisiae*. Methods in Molecular Biology, 1995. **47**(Electroporation Protocols for Microorganisms): p. 81-91.
6. Herman, P., et al., *Electroporative adjustment of pH in living yeast cells: ratiometric fluorescence pH imaging*. Journal of Fluorescence, 2005. **15**(5): p. 763-768.
7. Luo, C., et al., *Picoliter-volume aqueous droplets in oil: electrochemical detection and yeast cell electroporation*. Electrophoresis, 2006. **27**(10): p. 1977-1983.
8. Firon, A., et al., *Characterization of essential genes by parasexual genetics in the human fungal pathogen Aspergillus fumigatus: impact of genomic rearrangements associated with electroporation of DNA*. Genetics, 2002. **161**(3): p. 1077-1087.
9. Lakrod, K., C. Chaisrisook, and D.Z. Skinner, *Expression of pigmentation genes following electroporation of albino Monascus purpureus*. Journal of Industrial Microbiology & Biotechnology, 2003. **30**(6): p. 369-374.

10. Santos, M.A., et al., *Insertional mutagenesis in the vitamin B2 producer fungus Ashbya gossypii*. *Methods in Biotechnology*, 2005. **18**(Microbial Processes and Products): p. 283-300.
11. Taketo, A., *RNA transfection of Escherichia coli by electroporation*. *Biochimica et Biophysica Acta, Gene Structure and Expression*, 1989. **1007**(1): p. 127-9.
12. Rhee, M.S., et al., *Development of plasmid vector and electroporation condition for gene transfer in sporogenic lactic acid bacterium, Bacillus coagulans*. *Plasmid*, 2007. **58**(1): p. 13-22.
13. Jaroszeski, M.J., et al., *Drug and gene delivery to cells using aspirin and acetic acid*. 2007, (University of South Florida, USA). WO. p. 22pp.
14. Widera, G. and D. Rabussay, *Electroporation mediated drug & DNA delivery in oncology and gene therapy*. *Drug Delivery Technology*, 2002. **2**(3): p. 34,36-40.
15. Teissie, J., et al., *Recent biotechnological developments of electropulsation. A prospective review*. *Bioelectrochemistry*, 2002. **55**(1-2): p. 107-112.
16. Eksioglu-Demiralp, E., et al., *A method for functional evaluation of caspase activation pathways in intact lymphoid cells using electroporation-mediated protein delivery and flow cytometric analysis*. *Journal of Immunological Methods*, 2003. **275**(1-2): p. 41-56.
17. Gharney-Tagoe, E., et al., *Electroporation-mediated uptake of macromolecules and recovery of model intestinal epithelia*. *Proceedings - 28th International Symposium on Controlled Release of Bioactive Materials and 4th Consumer & Diversified Products Conference*, San Diego, CA, United States, June 23-27, 2001, 2001. **2**: p. 1013-1014.
18. Regnier, V., et al., *Mechanisms of a phosphorothioate oligonucleotide delivery by skin electroporation*. *International Journal of Pharmaceutics*, 1999. **184**(2): p. 147-156.
19. Javorovic, M., et al., *RNA Transfer by Electroporation into Mature Dendritic Cells Leading to Reactivation of Effector-Memory Cytotoxic T Lymphocytes: A Quantitative Analysis*. *Molecular Therapy*, 2005. **12**(4): p. 734-743.
20. Wells, D.J., *Gene Therapy Progress and Prospects: electroporation and other physical methods*. *Gene Therapy*, 2004. **11**(18): p. 1363-1369.
21. Barrau, C., J. Teissie, and B. Gabriel, *Osmotically induced membrane tension facilitates the triggering of living cell electroporabilization*. *Bioelectrochemistry*, 2004. **63**(1-2): p. 327-332.

22. Gimsa, J. and D. Wachner, *Analytical description of the transmembrane voltage induced on arbitrarily oriented ellipsoidal and cylindrical cells*. Biophysical Journal, 2001. **81**(4): p. 1888-1896.
23. Maswiwat, K., et al., *Simplified equations for the transmembrane potential induced in ellipsoidal cells of rotational symmetry*. Journal of Physics D-Applied Physics, 2007. **40**(3): p. 914-923.
24. Bernhardt, J. and H. Pauly, *On the generation of potential differences across the membranes of ellipsoidal cells in an alternating electrical field*. Biophysik, 1973. **10**(3): p. 89-98.
25. Teissie, J., M. Golzio, and M.P. Rols, *Mechanisms of cell membrane electropermeabilization: A minireview of our present (lack of ?) knowledge*. Biochimica et Biophysica Acta, General Subjects, 2005. **1724**(3): p. 270-280.
26. Gross, D., L.M. Loew, and W.W. Webb, *Optical imaging of cell membrane potential changes induced by applied electric fields*. Biophys J, 1986. **50**(2): p. 339-48.
27. Teissie, J. and M.P. Rols, *An experimental evaluation of the critical potential difference inducing cell membrane electropermeabilization*. Biophys J, 1993. **65**(1): p. 409-13.
28. Hibino, M., H. Itoh, and K. Kinoshita, Jr., *Time courses of cell electroporation as revealed by submicrosecond imaging of transmembrane potential*. Biophysical Journal, 1993. **64**(6): p. 1789-800.
29. Kotnik, T., D. Miklavcic, and T. Slivnik, *Time course of transmembrane voltage induced by time-varying electric fields - a method for theoretical analysis and its application*. Bioelectrochemistry and Bioenergetics, 1998. **45**(1): p. 3-16.
30. Golzio, M., J. Teissie, and M.-P. Rols, *Direct visualization at the single-cell level of electrically mediated gene delivery*. Proceedings of the National Academy of Sciences of the United States of America, 2002. **99**(3): p. 1292-1297.
31. Rols, M.-P., *Electropermeabilization, a physical method for the delivery of therapeutic molecules into cells*. Biochimica et Biophysica Acta, Biomembranes, 2006. **1758**(3): p. 423-428.
32. Kinoshita, K., Jr. and T.Y. Tsong, *Voltage-induced conductance in human erythrocyte membranes*. Biochimica et Biophysica Acta, Biomembranes, 1979. **554**(2): p. 479-97.
33. Vernier, P.T., Y. Sun, and A. Gundersen Martin, *Nanoelectropulse-driven membrane perturbation and small molecule permeabilization*. BMC Cell Biol, 2006. **7**: p. 37.

34. Beebe, S.J., et al., *Diverse Effects of Nanosecond Pulsed Electric Fields on Cells and Tissues*. DNA and Cell Biology, 2003. **22**(12): p. 785-796.
35. Rols, M.-P. and J. Teissie, *Electropermeabilization of mammalian cells to macromolecules: control by pulse duration*. Biophysical Journal, 1998. **75**(3): p. 1415-1423.
36. Rols, M.P. and J. Teissie, *Electropermeabilization of mammalian cells: quantitative analysis of the phenomenon*. Biophysical Journal, 1990. **58**(5): p. 1089-98.
37. Bilska, A.O., K.A. DeBruin, and W. Krassowska, *Theoretical modeling of the effects of shock duration, frequency, and strength on the degree of electroporation*. Bioelectrochemistry, 2000. **51**(2): p. 133-143.
38. Kotnik, T., et al., *Cell membrane electropermeabilization by symmetrical bipolar rectangular pulses. Part I. Increased efficiency of permeabilization*. Bioelectrochemistry, 2001. **54**(1): p. 83-90.
39. Tekle, E., R.D. Astumian, and P.B. Chock, *Electroporation by using bipolar oscillating electric field: an improved method for DNA transfection of NIH 3T3 cells*. Proceedings of the National Academy of Sciences of the United States of America, 1991. **88**(10): p. 4230-4.
40. Kotnik, T., D. Miklavcic, and L.M. Mir, *Cell membrane electropermeabilization by symmetrical bipolar rectangular pulses. Part II. Reduced electrolytic contamination*. Bioelectrochemistry, 2001. **54**(1): p. 91-95.
41. Kotnik, T., et al., *Role of pulse shape in cell membrane electropermeabilization*. Biochimica et Biophysica Acta, Biomembranes, 2003. **1614**(2): p. 193-200.
42. Pucihar, G., et al., *Electropermeabilization of dense cell suspensions*. Eur Biophys J, 2007. **36**(3): p. 173-85.
43. Canatella, P.J., et al., *Quantitative study of electroporation-mediated molecular uptake and cell viability*. Biophysical Journal, 2001. **80**(2): p. 755-764.
44. Sukhorukov, V.L., et al., *DNA, protein, and plasma-membrane incorporation by arrested mammalian cells*. Journal of Membrane Biology, 1994. **142**(1): p. 77-92.
45. Sachs, H.G., P.J. Stambrook, and J.D. Ebert, *Changes in membrane potential during the cell cycle*. Exp Cell Res, 1974. **83**(2): p. 362-6.
46. Golzio, M., J. Teissie, and M.-P. Rols, *Cell synchronization effect on mammalian cell permeabilization and gene delivery by electric field*. Biochimica et Biophysica Acta, Biomembranes, 2002. **1563**(1-2): p. 23-28.

47. Dorella, F.A., et al., *An improved protocol for electrotransformation of Corynebacterium pseudotuberculosis*. Veterinary Microbiology, 2006. **114**(3-4): p. 298-303.
48. Szostkova, M., D. Horakova, and M. Nemeč, *The influence of the growth phase of enteric bacteria on electrotransformation with plasmid DNA*. Folia Microbiologica, 1999. **44**(2): p. 177-180.
49. Tryfona, T. and M.T. Bustard, *Enhancement of biomolecule transport by electroporation: a review of theory and practical application to transformation of Corynebacterium glutamicum*. Biotechnology and Bioengineering, 2006. **93**(3): p. 413-423.
50. Muraji, M., W. Tatebe, and H. Berg, *The influence of extracellular alkali and alkaline-earth ions on electropermeation of Saccharomyces cerevisiae*. Bioelectrochemistry and Bioenergetics, 1998. **46**(2): p. 293-295.
51. Rao, K.V., K.S. Rathore, and T.K. Hodges, *Physical, chemical and physiological parameters for electroporation-mediated gene delivery into rice protoplasts*. Transgenic Research, 1995. **4**(6): p. 361-68.
52. Djuzenova, C.S., et al., *Effect of medium conductivity and composition on the uptake of propidium iodide into electropermeabilized myeloma cells*. Biochimica et Biophysica Acta, Biomembranes, 1996. **1284**(2): p. 143-152.
53. Loeffblom, J., et al., *Optimization of electroporation-mediated transformation: Staphylococcus carnosus as model organism*. Journal of Applied Microbiology, 2007. **102**(3): p. 736-747.
54. Ohshima, T. and M. Sato, *Bacterial sterilization and intracellular protein release by a pulsed electric field*. Advances in Biochemical Engineering/Biotechnology, 2004. **90**(Recent Progress of Biochemical and Biomedical Engineering in Japan I): p. 113-133.
55. Gallo, S.A., et al., *Temperature-dependent electrical and ultrastructural characterizations of porcine skin upon electroporation*. Biophysical Journal, 2002. **82**(1, Pt. 1): p. 109-119.
56. Wards, B.J. and D.M. Collins, *Electroporation at elevated temperatures substantially improves transformation efficiency of slow-growing mycobacteria*. FEMS Microbiology Letters, 1996. **145**(1): p. 101-105.
57. Golzio, M., M.P. Rols, and J. Teissie, *In vitro and in vivo electric field-mediated permeabilization, gene transfer, and expression*. Methods, 2004. **33**(2): p. 126-135.

58. Rols, M.P., et al., *Temperature effects on electrotransfection of mammalian cells*. Nucleic Acids Research, 1994. **22**(3): p. 540.
59. DeBruin, K.A. and W. Krassowska, *Modeling electroporation in a single cell. I. Effects of field strength and rest potential*. Biophysical Journal, 1999. **77**(3): p. 1213-1224.
60. Freeman, S.A., M.A. Wang, and J.C. Weaver, *Theory of electroporation of planar bilayer membranes: predictions of the aqueous area, change in capacitance, and pore-pore separation*. Biophysical Journal, 1994. **67**(1): p. 42-56.
61. Weaver, J.C. and R.A. Mintzer, *Decreased bilayer stability due to transmembrane potentials*. Physics Letters A, 1981. **86A**(1): p. 57-9.
62. Pastushenko, V.F., Y.A. Chizmadzhev, and V.B. Arakelyan, *Electric breakdown of bilayer lipid membranes. II. Calculation of the membrane lifetime in the steady-state diffusion approximation*. Bioelectrochemistry and Bioenergetics, 1979. **6**(1): p. 53-62.
63. Escoffre, J.M., et al., *Membrane perturbation by an external electric field: a mechanism to permit molecular uptake*. European Biophysics Journal, 2007. **36**(8): p. 973-983.
64. Vasilkoski, Z., et al., *Membrane electroporation: The absolute rate equation and nanosecond time scale pore creation*. Physical Review E: Statistical, Nonlinear, and Soft Matter Physics, 2006. **74**(2-1): p. 021904/1-021904/12.
65. Tieleman, D.P., *Computer simulations of transport through membranes: passive diffusion, pores, channels and transporters*. Clinical and Experimental Pharmacology and Physiology, 2006. **33**(10): p. 893-903.
66. Tarek, M., *Membrane electroporation: A molecular dynamics simulation*. Biophysical Journal, 2005. **88**(6): p. 4045-4053.
67. Vasilkoski, Z., *The effect of electric fields on lipid membranes*. Los Alamos National Laboratory, Preprint Archive, Physics, 2006: p. 1-10, arXiv:physics/0701013.
68. Powell, K.T. and J.C. Weaver, *Transient aqueous pores in bilayer membranes: a statistical theory*. Bioelectrochemistry and Bioenergetics, 1986. **15**(2): p. 221-227.
69. Joshi, R.P., et al., *Improved energy model for membrane electroporation in biological cells subjected to electrical pulses*. Phys Rev E Stat Nonlin Soft Matter Phys, 2002. **65**(4 Pt 1): p. 041920.

70. Chang, D.C. and T.S. Reese, *Changes in membrane structure induced by electroporation as revealed by rapid-freezing electron microscopy*. Biophys J, 1990. **58**(1): p. 1-12.
71. Weaver, J.C., *Electroporation of cells and tissues*. IEEE Transactions on Plasma Science, 2000. **28**(1): p. 24-33.
72. Shil, P., S. Bidaye, and P.B. Vidyasagar, *Analyzing the effects of surface distribution of pores in cell electroporation for a cell membrane containing cholesterol*. Los Alamos National Laboratory, Preprint Archive, Physics, 2007: p. 1-11, arXiv:0710 3081v1 [physics bio-ph].
73. Krassowska, W. and P.D. Filev, *Modeling electroporation in a single cell*. Biophysical Journal, 2007. **92**(2): p. 404-417.
74. Agrawal, A., *Electroporating single cells*. Analytical Chemistry, 2001. **73**(17): p. 474A.
75. Lundqvist, J.A., et al., *Altering the biochemical state of individual cultured cells and organelles with ultramicroelectrodes*. Proceedings of the National Academy of Sciences of the United States of America, 1998. **95**(18): p. 10356-10360.
76. Ryttsen, F., et al., *Characterization of single-cell electroporation by using patch-clamp and fluorescence microscopy*. Biophysical Journal, 2000. **79**(4): p. 1993-2001.
77. Aberg, M.A.I., et al., *Selective introduction of antisense oligonucleotides into single adult CNS progenitor cells using electroporation demonstrates the requirement of STAT3 activation for CNTF-induced gliogenesis*. Molecular and Cellular Neuroscience, 2001. **17**(3): p. 426-443.
78. Karlsson, M., et al., *Electroinjection of Colloid Particles and Biopolymers into Single Unilamellar Liposomes and Cells for Bioanalytical Applications*. Analytical Chemistry, 2000. **72**(23): p. 5857-5862.
79. Haas, K., et al., *Single-cell electroporation for gene transfer in vivo*. Neuron, 2001. **29**(3): p. 583-591.
80. Haas, K., et al., *Targeted electroporation in Xenopus tadpoles in vivo - from single cells to the entire brain*. Differentiation, 2002. **70**(4-5): p. 148-154.
81. Rae, J.L. and R.A. Levis, *Single-cell electroporation*. Pfluegers Archiv, 2002. **443**(4): p. 664-670.
82. Rathenberg, J., T. Nevian, and V. Witzemann, *High-efficiency transfection of individual neurons using modified electrophysiology techniques*. J Neurosci Methods, 2003. **126**(1): p. 91-8.
83. Bae, C. and P.J. Butler, *Automated single-cell electroporation*. BioTechniques, 2006. **41**(4): p. 399-400,402.

84. Nevian, T. and F. Helmchen, *Calcium indicator loading of neurons using single-cell electroporation*. Pfluegers Archiv, 2007. **454**(4): p. 675-688.
85. Graham, L.J., et al., *A method of combined single-cell electrophysiology and electroporation*. Journal of Neuroscience Methods, 2007. **160**(1): p. 69-74.
86. Sorensen, S.A. and E.W. Rubel, *The level and integrity of synaptic input regulates dendrite structure*. Journal of Neuroscience, 2006. **26**(5): p. 1539-1550.
87. Bestman Jennifer, E., et al., *In vivo single-cell electroporation for transfer of DNA and macromolecules*. Nat Protoc, 2006. **1**(3): p. 1268-73.
88. Saheki, Y., et al., *A new approach to inhibiting astrocytic IP3-induced intracellular calcium increase in an astrocyte-neuron co-culture system*. Brain Research, 2005. **1055**(1-2): p. 196-201.
89. Uesaka, N., et al., *Interplay between laminar specificity and activity-dependent mechanisms of thalamocortical axon branching*. Journal of Neuroscience, 2007. **27**(19): p. 5215-5223.
90. Uesaka, N., et al., *Activity dependence of cortical axon branch formation: a morphological and electrophysiological study using organotypic slice cultures*. J Neurosci, 2005. **25**(1): p. 1-9.
91. Nolkranz, K., et al., *Electroporation of single cells and tissues with an electrolyte-filled capillary*. Analytical Chemistry, 2001. **73**(18): p. 4469-4477.
92. Nolkranz, K., et al., *Functional screening of intracellular proteins in single cells and in patterned cell arrays using electroporation*. Analytical Chemistry, 2002. **74**(16): p. 4300-4305.
93. Olofsson, J., et al., *Scanning electroporation of selected areas of adherent cell cultures*. Analytical Chemistry (Washington, DC, United States), 2007. **79**(12): p. 4410-4418.
94. Huang, Y. and B. Rubinsky, *Microfabricated electroporation chip for single cell membrane permeabilization*. Sensors and Actuators, A: Physical, 2001. **A89**(3): p. 242-249.
95. Huang, Y. and B. Rubinsky, *Micro-Electroporation: Improving the Efficiency and Understanding of Electrical Permeabilization of Cells*. Biomedical Microdevices, 1999. **2**(2): p. 145-150.
96. Diaz-Rivera Ruben, E. and B. Rubinsky, *Electrical and thermal characterization of nanochannels between a cell and a silicon based micro-pore*. Biomed Microdevices, 2006. **8**(1): p. 25-34.

97. Kurosawa, O., et al., *Electroporation through a micro-fabricated orifice and its application to the measurement of cell response to external stimuli*. Measurement Science and Technology, 2006. **17**(12): p. 3127-3133.
98. Sarkar, A., et al., *A low voltage single cell electroporator with a microfabricated sense-porate aperture*. IEEE International Conference on Micro Electro Mechanical Systems, Technical Digest, 17th, Maastricht, Netherlands, Jan. 25-29, 2004, 2004: p. 375-378.
99. Khine, M., et al., *A single cell electroporation chip*. Lab on a Chip, 2005. **5**(1): p. 38-43.
100. Seo, J., et al., *Integrated multiple patch-clamp array chip via lateral cell trapping junctions*. Applied Physics Letters, 2004. **84**(11): p. 1973-1975.
101. Khine, M., et al., *Single-cell electroporation arrays with real-time monitoring and feedback control*. Lab on a Chip, 2007. **7**(4): p. 457-462.
102. Wang, H.-Y. and C. Lu, *Electroporation of Mammalian Cells in a Microfluidic Channel with Geometric Variation*. Analytical Chemistry, 2006. **78**(14): p. 5158-5164.
103. Wang, H.-Y. and C. Lu, *High-throughput and real-time study of single cell electroporation using microfluidics: effects of medium osmolarity*. Biotechnology and Bioengineering, 2006. **95**(6): p. 1116-1125.
104. He, H., D.C. Chang, and Y.-K. Lee, *Micro pulsed radio-frequency electroporation chips*. Bioelectrochemistry, 2006. **68**(1): p. 89-97.
105. Yang, F., et al., *Parametric study of pulsed radio-frequency electroporation on microchips at the single-cell level*. Special Publication - Royal Society of Chemistry, 2004. **297**(Micro Total Analysis Systems 2004, Volume 2): p. 79-81.
106. He, H., D.C. Chang, and Y.-K. Lee, *Using a micro electroporation chip to determine the optimal physical parameters in the uptake of biomolecules in HeLa cells*. Bioelectrochemistry, 2007. **70**(2): p. 363-368.
107. Rojas-Chapana, J., et al., *Multi-walled carbon nanotubes for plasmid delivery into Escherichia coli cells*. Lab on a Chip, 2005. **5**(5): p. 536-539.
108. Sweedler, J.V. and E.A. Arriaga, *Single cell analysis*. Analytical and Bioanalytical Chemistry, 2007. **387**(1): p. 1-2.
109. Lu, X., et al., *Recent developments in single-cell analysis*. Analytica Chimica Acta, 2004. **510**(2): p. 127-138.

110. Zhang, H. and W.R. Jin, *Single-cell analysis by intracellular immuno-reaction and capillary electrophoresis with laser-induced fluorescence detection*. Journal of Chromatography A, 2006. **1104**(1-2): p. 346-351.
111. Troyer, K.P. and R.M. Wightman, *Dopamine transport into a single cell in a picoliter vial*. Analytical Chemistry, 2002. **74**(20): p. 5370-5375.
112. Lenihan, J.S., et al., *Microfabrication of screen-printed nanoliter vials with embedded surface-modified electrodes*. Analytical and Bioanalytical Chemistry, 2007. **387**(1): p. 259-265.
113. Zudans, I., et al., *Numerical calculations of single-cell electroporation with an electrolyte-filled capillary*. Biophysical Journal, 2007. **92**(10): p. 3696-3705.
114. Agarwal, A., et al., *Simultaneous Maximization of Cell Permeabilization and Viability in Single-Cell Electroporation Using an Electrolyte-Filled Capillary*. Analytical Chemistry, 2007. **79**(1): p. 161-167.
115. Lambie, B.A., et al., *Experimentally determining the iR drop in solution at carbon fiber microelectrodes with current interruption and application to single-cell electroporation*. Analytical Chemistry, 2007. **79**(10): p. 3771-3778.
116. Langmuir, M.E., et al., *New thiol active fluorophores for intracellular thiols and glutathione measurement*. Fluorescence Microscopy and Fluorescent Probes, [Based on the Proceedings of the Conference on Fluorescence Microscopy and Fluorescent Probes], Prague, June 25-28, 1995, 1996: p. 229-233.
117. Kagan, V.E., et al., *Pro-oxidant and antioxidant mechanisms of etoposide in HL-60 cells: role of myeloperoxidase*. Cancer Research, 2001. **61**(21): p. 7777-7784.
118. Hamill, O.P., et al., *Improved patch-clamp techniques for high-resolution current recording from cells and cell-free membrane patches*. Pflugers Archiv : European journal of physiology, 1981. **391**(2): p. 85-100.
119. Neher, E., B. Sakmann, and J.H. Steinbach, *The extracellular patch clamp: a method for resolving currents through individual open channels in biological membranes*. Pfluegers Archiv, 1978. **375**(2): p. 219-28.
120. Liminga, G., et al., *On the mechanism underlying calcein-induced cytotoxicity*. European Journal of Pharmacology, 1999. **383**(3): p. 321-329.
121. Liminga, G., et al., *Apoptosis induced by calcein acetoxymethyl ester in the human histiocytic lymphoma cell line U-937 GTB*. Biochemical Pharmacology, 2000. **60**(12): p. 1751-1759.

122. Liminga, G., et al., *Cytotoxic Effect of Calcein Acetoxymethyl Ester on Human Tumor-Cell Lines - Drug-Delivery by Intracellular Trapping*. *Anti-Cancer Drugs*, 1995. **6**(4): p. 578-585.
123. Hayashi, S., et al., *Modification of thermosensitivity by amrubicin or amrubicinol in human lung adenocarcinoma A549 cells and the kinetics of apoptosis and necrosis induction*. *International Journal of Molecular Medicine*, 2005. **16**(3): p. 381-387.
124. Moris, G., et al., *Dinucleoside tetrphosphate variations in cultured tumor cells during their cell cycle and growth*. *Biochimie*, 1987. **69**(11-12): p. 1217-25.
125. Wu, F., et al., *Cell cycle-dependent expression of cyclin D1 and a 45 kD protein in human A549 lung carcinoma cells*. *American Journal of Respiratory Cell and Molecular Biology*, 1994. **10**(4): p. 437-47.